Influence of basement rocks on fluid evolution during multiphase deformation: the example of the Estamariu thrust in the Pyrenean Axial Zone

Daniel Muñoz-López[1], Gemma Alías[1], David Cruset[2], Irene Cantarero[1], Cédric M. John[3], Anna Travé[1]

[1]Department de Mineralogia, Petrologia i Geologia Aplicada. Facultat de Ciències de la Terra, Universitat de Barcelona (UB), C/ Martí i Franquès s/n, 08028 Barcelona, Spain.
[2]Group of Dynamics of the Lithosphere (GDL), Geosciences Barcelona, GEO3BCN-CSIC, Lluís Solé i Sabarís s/n, 08028 Barcelona, Spain.
[3]Department of Earth Science and Engineering, Imperial College London, London SW7 2BP, UK.

Correspondence to: Daniel Muñoz-López (munoz-lopez@ub.edu)

Abstract. Calcite veins precipitated in the Estamariu thrust during two tectonic events are studied in order to: (i) decipher the temporal and spatial relationships between deformation and fluid migration in a long-lived thrust and, (ii) determine the influence of basement rocks on the fluid chemistry during deformation. Structural and petrological observations constrain the relative timing of fluid migration and vein formation, whilst geochemical analyses (δ^{13}C, δ^{18}O, ^{87}Sr/^{86}Sr, clumped isotope thermometry and elemental composition) applied to the related calcite cements and host rocks indicate the fluid origin, pathways and extent of fluid-rock interaction. The first tectonic event, recorded by calcite cements Cc1a and Cc2, is attributed to the Alpine reactivation of the Estamariu thrust. Analytical data indicates that these cements precipitated from heated meteoric fluids (temperatures in the range of 50 to 100 ºC) that had interacted with basement rocks (^{87}Sr/^{86}Sr > 0.71) before upflowing through the thrust zone. The second tectonic event, attributed to the Neogene extension, is characterized by the reactivation of the Estamariu thrust and the formation of normal faults and shear fractures sealed by calcite cements Cc3, Cc4 and Cc5. Analytical data indicates that cements Cc3 and Cc4 precipitated from hydrothermal fluids (temperatures between 130 and 210 ºC and between 100 and 170 ºC, respectively) that had interacted with basement rocks (^{87}Sr/^{86}Sr > 0.71) and been expelled through fault zones during deformation. In contrast, cement Cc5 probably precipitated from meteoric waters that likely percolated from the surface through small shear fractures.

The comparison between our results and already published data in other structures from the Southern Pyrenees suggests that regardless of the origin of the fluids and the tectonic context, basement rocks have a significant influence on the fluid chemistry, particularly on the ^{87}Sr/^{86}Sr ratio. Accordingly, the cements precipitated from fluids that have interacted with basement rocks have significantly higher ^{87}Sr/^{86}Sr ratios (> 0.710) with respect to those precipitated from fluids that have interacted with the sedimentary cover (< 0.710), which involves younger and less radiogenic rocks.

1 Introduction

Deformation associated with crustal shortening is mainly accommodated by thrust faulting and related fault zone structures (Mouthereau et al., 2014; Muñoz, 1992; Sibson, 1994). Successive faulting may occur and favourably oriented structures may undergo reactivation during different tectonic events in a long-lived orogenic belt (Cochelin et al., 2018; Sibson, 1995). The

35 reactivation of faults may produce changes in the hydraulic behaviour of fault zones as well as in the origin and regime of fluids circulating through them (Arndt et al., 2014; Barker and Cox, 2011; Cantarero et al., 2018; Cruset et al., 2018; Lacroix et al., 2018; Travé et al., 2007). Consequently, constraining the timing of deformation and fluid migration is essential to better understand the main factors leading to the current configuration of a mountain belt, its evolution through time, and the mobilization of different fluids during successive deformation events (Baques et al., 2012; Crespo-Blanc et al., 1995; Faÿ-

40 Gomord et al., 2018; Fitz-Diaz et al., 2011; Lacroix et al., 2014). Understanding basin-scale fluid flow is of primary importance to reconstruct the diagenetic history of a sedimentary basin, as fluids take part in a wide range of geological processes including precipitation of new mineral phases, dolomitization and petroleum migration, among others (Barker et al., 2009; Foden, 2001; Fontana et al., 2014; Gomez-Rivas et al., 2014; Martín-Martín et al., 2015; Mozafari et al., 2019; Piessens et al., 2002). Due to the economic interest of these processes, in particular related to oil and ore deposits exploration, CO_2 sequestration, seismic

45 activity and water management, many researchers have addressed the study of the relationship between deformation and fluid migration (Beaudoin et al., 2014; Breesch et al., 2009; Cox, 2007; Dewever et al., 2013; Gasparrini et al., 2013; Muñoz-López et al., 2020; Suchy et al., 2000; Travé et al., 2009; Voicu et al., 2000; Warren et al., 2014).

In the Pyrenees, the basement rocks from the Axial Zone are affected by numerous fault systems related to the Variscan orogeny (Late Paleozoic) but reactivated during the Pyrenean compression (Late Cretaceous to Oligocene) (Cochelin et al.,

50 2018; Poblet, 1991). However, no real consensus exists about the influence of the Alpine deformation on the basement rocks and the age of basement-involved structures is still debated (Cochelin et al., 2018; García-Sansegundo et al., 2011). As a consequence, the relationships between deformation and fluid flow have been widely focused on structures from the Mesozoic and Cenozoic cover (Beaudoin et al., 2015; Crognier et al., 2018; Cruset et al., 2016, 2018, 2020a; Lacroix et al., 2011, 2014; Martinez Casas et al., 2019; Muñoz-López et al., 2020; Nardini et al., 2019; Travé et al., 1997, 1998, 2000), where the timing

55 of deformation and thrust emplacement is well-constrained (Cruset et al., 2020b; Vergés, 1993; Vergés and Muñoz, 1990). In contrast, few studies, only concentrated along the Gavarnie thrust system, have examined the relationship between deformation and fluid migration in the Paleozoic basement (Banks et al., 1991; Grant et al., 1990; Henderson and McCaig, 1996; McCaig et al., 2000a, 1995; Rye and Bradbury, 1988; Trincal et al., 2017). Another important aspect of studying the fault-fluid system is related to the heat flow and the influence of faults on the development of geothermal systems (Faulds et al., 2010; Grasby

60 and Hutcheon, 2001; Liotta et al., 2010; Rowland and Sibson, 2004). Particularly, in the NE part of the Iberian Peninsula (including the Pyrenees and the Catalan Coastal Ranges), the presence of high-permeability Neogene extensional faults, acting as conduits for upward migration, provide efficient pathways for hydrothermal fluids to flow from deeper to shallower crustal levels (Carmona et al., 2000; Fernàndez and Banda, 1990; Taillefer et al., 2017, 2018). In this sense, understanding the fault-

fluid system evolution and the relative timing of hydrothermal fluid migration is of great importance to characterize the potential geothermal resources of this area.

In this contribution, we report the temporal and spatial relationships between deformation and fluid migration in a long-lived Variscan thrust deforming basement rocks in the Pyrenean Axial Zone. For this purpose, we combine structural, petrological and geochemical analyses of calcite veins precipitated in the Estamariu thrust during two reactivation episodes related to the Alpine compression (Late Cretaceous to Oligocene) and the Neogene extension. Structural and petrological observations allow us to unravel the relative timing of fluid migration and vein formation in relation to the involved tectonic events. The geochemistry of the vein cements and related host rocks provides information on the fluid origin, pathways and extent of fluid-rock interaction during deformation. Therefore, the main objectives of this paper are: (i) to constrain the relative timing of vein formation and fluid migration; (ii) to determine the fluid origin and pathways during successive compressional and extensional deformation phases; (iii) to assess the influence of basement rocks on the chemistry of fluids circulating during deformation; and (iv) to provide insights into the fluid flow at regional scale in the NE part of the Iberian Peninsula, where the presence of hydrothermal fluids has been reported from Neogene times to present.

2 Geological setting

The Pyrenees constitute an asymmetric and doubly verging orogenic belt that resulted from the Alpine (Late Cretaceous to Oligocene) convergence between the Iberian and European plates (Choukroune, 1989; Muñoz, 1992; Roure et al., 1989; Sibuet et al., 2004; Srivastava et al., 1990; Vergés and Fernàndez, 2012). The Pyrenean structure consists of a central antiformal stack of basement-involved rocks from the Axial Zone, flanked by two oppositely verging fold-and-thrust belts and their associated foreland basins (Muñoz, 1992; Muñoz et al., 1986) (Fig. 1A). The Pyrenean Axial Zone has been deformed by successive Variscan, Alpine and Neogene phases (Saura and Teixell, 2006). In the eastern Axial Pyrenees, an E-W to ENE-WSW fault system developed during the Neogene extension (Roca, 1996; Roca and Guimerà, 1992; Vergés et al., 2002). The main fault, La Tet fault, has associated a set of E-W extensional basins such as La Cerdanya, Conflent, La Seu d'Urgell and the Cerc basins (Cabrera et al., 1988; Roca, 1996). The Cerc basin consists of a Stephano-Permian accumulation of volcanic rocks discordantly overlying Cambro-Ordovician materials. This basin is thrusted in its eastern limit by the Estamariu thrust, whereas the northern and southern boundaries correspond to two Neogene extensional faults, La Seu d'Urgell fault and the Ortedó fault, respectively (Hartevelt, 1970; Roca, 1996; Saura, 2004) (Fig. 1B, C). In the NW part of the basin, the limit between the Stephano-Permian unit and the Upper Ordovician sequence corresponds to a Stephano-Permian extensional fault formed coevally with the deposition of the volcanic sequence (Saura, 2004). This fault was reactivated during the latest stages of the Neogene extension (Saura, 2004) and is here referred as the Sant Antoni fault (Fig. 1C).

The Estamariu thrust is a basement-involved reverse fault originated during the Variscan orogeny with a minimum displacement of 27 km (Poblet, 1991). However, in its southwestern termination, it juxtaposes the Devonian Rueda Formation against the Stephano-Permian Erill Castell Formation. The Erill Castell Formation developed during the late to post-orogenic

collapse of the Variscan belt (Lago et al., 2004; Martí, 1991, 1996; Ziegler, 1988), evidencing the reactivation of the Estamariu thrust during the Alpine Orogeny (Poblet, 1991; Saura, 2004). Rocks cropping out around the Estamariu thrust and the Cerc basin range from Upper Ordovician to Miocene (Fig. 1C). However, due to the complex structural setting, the stratigraphic record is discontinuous and only Upper Ordovician, Devonian, Stephano-Permian and Neogene rocks are present in the study

100 area. The basement lithologies consists of Upper Ordovician and Devonian metasedimentary rocks affected by multiscale folds and related pervasive axial plane regional foliation (Bons, 1988; Casas et al., 1989; Cochelin et al., 2018; Zwart, 1986). This deformation is linked to low-grade metamorphic conditions developed during the Variscan orogeny (Hartevelt, 1970; Poblet, 1991; Saura, 2004). The Upper Ordovician succession includes an alternation of shales, sandstones, conglomerates, quartzites and phyllites, and the Devonian sequence consists of an alternation of limestones and black slates (Rueda Formation) (Mey,

105 1967). The Stephano-Permian sequence developed during the late to post-orogenic extensional collapse of the Variscan belt and in the study area is represented by a volcanic and volcanoclastic unit (the Erill Castell Formation) (Martí, 1991; Mey et al., 1968), involving tuffs and ignimbrites at the base and andesites in the upper part (Martí, 1996; Saura and Teixell, 2006). Finally, the Neogene sequence is constituted of detrital and poorly lithified sediments, mainly shales, sandstones and conglomerates deposited during the Neogene extension associated with the opening of the NW Mediterranean Sea (Roca,

110 1996).

3 Methods

This study integrates a field compilation of structural data as well as petrological and geochemical analyses of calcite cements and related host rocks. The structural data includes the orientation of bedding, foliations, and fractures in addition to crosscutting relationships and kinematics. Such data were plotted in equal-area lower-hemisphere projections and different

115 fracture sets were stablished according to their type, strike, mineral infillings, and relative age deduced from crosscutting relationships. All these data were integrated in a schematic map and a cross-section of the Estamariu thrust and the Cerc basin (Fig. 2A, B and 3). Samples considered representative of the involved host rocks and all calcite vein generations observed in the different fracture sets and fault-related structures were selected for petrological and geochemical analyses. Thin sections of these samples were prepared and studied under a Zeiss Axiophot optical microscope and a Cold cathodoluminescence (CL)

120 microscope model 8200 Mk5-1 operating between 16–19 kV and 350 µA gun current.

The geochemical analyses have been performed in calcite cements and related host rocks in order to determine the origin, composition and temperature of the vein-forming fluids in addition to the extent of fluid-rock interaction. These analyses include: (i) stable isotope analyses in 37 calcite cements and the carbonate portion of the Devonian rocks, (ii) the elemental composition of twelve samples analyzed using a high resolution inductively coupled plasma-mass spectrometry (HR-ICP-

125 MS), (iii) the $^{87}Sr/^{86}Sr$ and $^{143}Nd/^{144}Nd$ ratios of eight representative samples, and, (iv) clumped isotope thermometry of calcite cements (three samples), which results were converted to temperatures applying the calibration method of (Kluge et al., 2015).

Calculated $\delta^{18}O_{fluid}$ values are expressed in ‰ with respect to the Vienna Standard Mean Ocean Water (VSMOW). Details of methods and procedures can be found in the supplementary data.

4 Results

4.1 Structure and associated calcite cements

The Estamariu thrust strikes N-S to NW-SE and dips between 40 and 70º towards the NE. It has a displacement of a few hundred meters and juxtaposes a Devonian alternation of limestones and shales in the hanging wall against Stephano-Permian andesites in the footwall (Poblet, 1991) (Fig. 2-4). The main slip plane is undulose and generates a 2 – 3 m thick thrust zone affecting both the hanging wall and footwall, but it is thicker in the hanging wall, up to 2.5 m thick. In the footwall the thrust zone is less than 1 m thick and has associated minor restricted thrust zones developed as subsidiary accommodation structures related to the main thrust fault (Fig. 2A, B). All kinematic indicators, including S-C structures and slickenlines, indicate reverse displacement towards the west.

The mesostructures and microstructures observed in the study area are described below according to their structural position in relation to the Estamariu thrust, that is, hanging wall, thrust zone and footwall (Fig. 3, 4). The relative timing of the different mesostructures and microstructures has been determined by means of crosscutting relationships and microstructural analysis.

4.1.1 Hanging wall

In the studied outcrops, the Devonian Rueda Formation is characterized by a well-bedded alternation of dark to light grey limestones with subordinate dark grey shales (S0) (Fig. 5A). Limestones are made up of encrinites, which consist of a bioclastic packstone formed essentially of crinoid stems (Fig. 5B). Under cathodoluminescence, encrinites show dark to bright orange colors (Fig. 5C). Devonian rocks form a decametric anticline oriented NW-SE with a well-developed axial plane foliation (S_1) concentrated in the pelitic intervals. S_1, which is oriented NNW-SSE, is a pervasive regional foliation dipping 30 to 55º towards the E and NE and is generally between 2 and 5 cm spaced. In the hinge of the anticline, bedding (S0) dips towards the SE and forms a high angle with S_1 (Fig. 2B and 5A), whereas in its eastern limb, the regional foliation (S_1) dips steeper than S0. These geometric relationships between bedding and foliation have been used to determine the fold type at great scale (i.e., as it is shown in Fig. 2B).

4.1.2 Thrust zone

The thrust zone consists of a deformation zone affecting both the hanging wall and the footwall. Within the hanging wall, the Devonian host rocks are still recognizable, but the intensity of deformation progressively increases towards the main thrust plane. This deformation consists of a penetrative thrust zone foliation (S_2), two generations of stylolites (e1, e2) and three generations of calcite veins (V0, V1a and V1b) (Fig. 3, 6). These structures are described below in chronological order.

The foliation within the thrust zone affecting the Devonian hanging wall (S_2) strikes NW-SE and dips 40 – 50º NE, similar to the regional foliation (S_1), but it is more closely spaced, generally between 0.2 and 1 cm (Fig. 6A, B). This observation points to a progressive transposition of the regional foliation within the thrust zone during thrusting. At mesoscale, S_2 has related shear surfaces (Ci) defining centimetric S-C-type structures, indicating again reverse kinematics (Fig. 6A).

160 Stylolites e1 have a wave-like shape and trend subparallel to the thrust zone foliation (S_2) (Fig. 6B, C). When present, these stylolites are very systematic exhibiting a spacing of 1 – 2 mm (Fig. 6C).

The first calcite vein generation (V0), only observed at microscopic scale (Fig. 6B, C), corresponds to up to 1 cm long and less than 1 mm thick veins cemented by blocky to elongated blocky calcite crystals featuring a dark-brown luminescence (cement Cc0). Veins V0 and stylolites e1 are perpendicular between them and show ambiguous crosscutting relationships. These

165 microstructures are concentrated into discontinuous fragments of the Devonian host rocks within the thrust zone. Calcite veins V1a crosscut the previous vein generation (V0) as well as the stylolites e1 and are developed within S_2 surfaces (Fig. 3, 6D). These veins are the most abundant, exhibit a white to brownish color in hand sample and are up to 10 cm long and 1 cm thick. The vein cement (Cc1a) is formed of up to 3-4 mm in size anhedral crystals displaying a blocky texture and a dark brown luminescence (Fig. 6E).

170 Stylolites e2, more abundant than stylolites e1, are up to 10 cm long and show spacing between 0.5 and 2 cm (Fig. 6D, F). These stylolites mainly correspond to sutured areas developed between the host rock and the calcite veins V1a and between foliation surfaces S_2.

Calcite veins V1b, up to 1 cm long and less than one mm thick, were also identified at microscopic scale (Fig. 6D, F). The vein cement (Cc1b) consists of up to 0.1 mm calcite crystals with a blocky texture and a bright yellow luminescence. These

175 veins postdate the previous V0 and V1a generations and trend perpendicular to stylolites e2.

Towards the fault plane, the thrust zone foliation S_2 is progressively more closely-spaced and stylolites e2 become more abundant (showing mm spacing) and exhibit ambiguous cross-cutting relationships with veins V1b (Fig. 6F). The main slip surface corresponds to a discrete plane that contains calcite slickensides (veins V2). The vein cement (Cc2) is milky white in hand sample and consists of up to 3 mm blocky to elongated blocky crystals (Fig. 6G) with a dull to bright orange luminescence

180 (Fig. 6H).

Deformation in the footwall is concentrated within the main thrust zone and subsidiary thrust zones and corresponds to the thrust zone foliation (S_2) and calcite veins V3 (Fig. 3). This foliation (S_2) strikes NW-SE, dips towards the NE and is mm to cm spaced (Fig. 7A). Calcite veins V3 are generally 1 – 2 cm thick and strike NW-SE. They are parallel or locally branch off cutting the S_2 planes in the subsidiary thrust zone (Fig. 7A, B). Outside the thrust zone, veins V3 are locally present but have

185 a NE-SW strike. These veins are mostly less than 1 m long and are spaced between a few cm and 50 cm. The vein cement (Cc3) is made up of a milky white calcite characterized by up to 3 mm long fibrous crystals oriented perpendicular to the vein walls (Fig. 7C). Locally, anhedral blocky crystals ranging in size from 0.1 to 1 mm are also present. This cement displays a bright yellow to bright orange luminescence (Fig. 7D).

4.1.3 Footwall

190 In the footwall, the Stephano-Permian Erill Castell Formation comprises massive, dark-greenish andesitic levels showing a rhythmic magmatic layering (Fig. 7E), which corresponds to a fluidal structure of the host rock. The local presence of pyroclastic and brecciated volcanoclastic levels is also ubiquitous mainly in the lower part of this sequence. Andesites are characterized by a porphyritic texture defined by a dark fine-grained spherulitic matrix partially devitrified and large zoned crystals of plagioclase (Fig. 7F), up to 2 – 3 cm long, and less abundant biotite and hornblende. These mafic phenocrystals are

195 systematically pseudomorphosed by clay minerals and frequently show evidence of oxidation and chloritization. Andesites are affected by E-W striking open joints (J1) dipping indistinctively towards the north and south (Fig. 7E). These joints locally trend parallel to the magmatic layering (Fig. 3).

Finally, as described above, the northern and southern limits of both the Cerc basin and the Estamariu thrust correspond to two Neogene extensional faults, La Seu d'Urgell and the Ortedó fault systems (Fig 1C). These faults are subvertical or steeply dip

200 towards the north. In the northern part, the slip plane of La Seu d'Urgell fault has not been observed and the limit between the Stephano-Permian rocks and the Neogene deposits is not well constrained due to the poor quality of the Neogene outcrops and the presence of Quaternary deposits. In the southern part, the Ortedó fault generates a several meter-thick dark greyish to brown fault zone, characterized by the presence of clay-rich incohesive fault rocks developed at the contact between Stephano-Permian and Upper Ordovician rocks. Related to these main fault systems, mesoscale normal faults commonly affect the

205 andesites within the Cerc basin. These faults are mainly E-W and locally NE-SW, are subvertical and dip indistinctly towards the N and S. Fault planes are locally mineralized with calcite cement (veins V4) and exhibit two striae set generations indicating dip-slip and strike-slip movements (Fig. 8A). The calcite cement (Cc4) consists of up to 2 mm blocky to elongated blocky crystals (Fig. 8B) with a homogeneous dark orange luminescence (Fig. 8C). On the other hand, the main Estamariu thrust zone is locally displaced by shear fractures (Fig. 8D) and a later set of shear bands (Cn) (Fig. 8E), both having an overall NNW-

210 SSE to NNE-SSW strike (Fig. 3) that indicate a minor normal displacement. Shear fractures are locally mineralized with calcite (veins V5). The vein cement consists of a greyish microsparite calcite cement (Cc5) (Fig. 8F-G).

4.2 Geochemistry of calcite cements and host rocks

The geochemistry ($\delta^{18}O$, $\delta^{13}C$, $\delta^{18}O_{fluid}$, $^{87}Sr/^{86}Sr$, $^{143}Nd/^{144}Nd$ and elemental composition) and the calculated temperature of precipitation of the different calcite cements Cc1a to Cc5 are described below. Veins V0 and V1b were only observed at

215 microscopic scale and their calcite cement Cc0 and Cc1b could not be sampled to perform these geochemical analyses.

The $\delta^{18}O$ and $\delta^{13}C$ isotopic composition of the carbonate fraction of the Devonian hanging wall and the different calcite cements (Cc1a to Cc5) are summarized in Table 1 and represented in Fig. 9. The micritic matrix of the Devonian packstone ranges in $\delta^{18}O$ values between -10.5 and -8.4 ‰VPDB and in $\delta^{13}C$ values between +1.5 and +2.8 ‰VPDB, whereas the calcite cements have a broader range of values depending on the cement generation (Fig. 9).

Calcite cement Cc1a has $\delta^{18}O$ values between -11.3 and -10.3 ‰VPDB and $\delta^{13}C$ values between +0.8 and +2.1 ‰VPDB. Cc2 is characterized by $\delta^{18}O$ values between -14.9 and -12.9 ‰VPDB and $\delta^{13}C$ values between -1.2 and +1.5 ‰VPDB. Cc3 has $\delta^{18}O$ values between -14.3 and -13.4 ‰VPDB and $\delta^{13}C$ values between -9.3 and -6.9 ‰VPDB. Cc4 exhibits $\delta^{18}O$ values between -13.8 and -13.4 ‰VPDB and $\delta^{13}C$ values between -7.4 and -7.2 ‰VPDB and Cc5 ranges in $\delta^{18}O$ between -8.1 and -5.7 ‰VPDB and in $\delta^{13}C$ between -8.2 and -3.8 ‰VPDB. The calcite cement Cc1a, precipitated in the fault zone affecting the Devonian hanging wall, has enriched $\delta^{13}C$ values, whilst the calcite cement within the fault plane (Cc2) exhibits either negative or positive $\delta^{13}C$ values and the calcite cements hosted in the Stephano-Permian andesites (Cc3 to Cc5) have more depleted $\delta^{13}C$ values (Fig. 9). In addition, calcite cements show a progressive depletion in $\delta^{18}O$ from Cc1a to Cc4, whereas Cc5 displays more enriched $\delta^{18}O$ values.

The obtained Δ_{47} values from clumped isotope thermometry were converted into temperatures and $\delta^{18}O_{fluid}$ (Table 1 and Fig. 10) using the equation of (Kluge et al., 2015) and (Vinet and Zhedanov, 2010), respectively. The calculated T and $\delta^{18}O_{fluid}$ for calcite cement Cc2 range between 50 and 100 ºC and between -6.4 and -0.3 ‰VSMOW, respectively. Cement Cc3 shows T and $\delta^{18}O_{fluid}$ in the range of 130 to 210 ºC and +4.3 to +12.1 ‰VSMOW, respectively. Cc4 exhibits T and $\delta^{18}O_{fluid}$ in the range of 100 to 170 ºC and +0.9 to +8.1 ‰VSMOW, respectively.

The $^{87}Sr/^{86}Sr$ ratio of calcite cements Cc1a to Cc5 and host rocks are reported in Table 1 and Fig. 11. Devonian limestones from the hanging wall have a $^{87}Sr/^{86}Sr$ ratio of 0.710663, whilst the Stephano-Permian andesites in the footwall exhibit a more radiogenic $^{87}Sr/^{86}Sr$ ratio of 0.743983. The calcite cements have more radiogenic $^{87}Sr/^{86}Sr$ ratios than the Devonian limestones but less radiogenic values than the Stephano-Permian andesites. This ratio ranges from 0.713018 to 0.714092 in Cc1a, is 0.718294 for Cc2, 0.714619 for Cc3, 0.717706 for Cc4 and 0.716923 for Cc5. These results are compared with already published data from synkinematic veins and deformed rocks in other Pyrenean structures developed in the basement and in the sedimentary cover during the Pyrenean compression (Fig. 11). This comparison shows that values obtained in this study are: 1) significantly more radiogenic than the values of marine carbonates and synkinematic veins precipitated in the sedimentary cover (i.e., in the South Pyrenean fault and thrust belt) and, 2) within the same range of values of synkinematic veins and deformed rocks in the Pyrenean basement (Axial Zone).

The analyzed samples for $^{143}Nd/^{144}Nd$ ratios in calcite cements and host rocks are reported in Table 1. However, due to the general low Nd concentrations in most of the analyzed calcite cements and the limited amount of powdered samples that were available, only calcite cement Cc5 and the andesite host rock (footwall) could be measured. Cc5 has a $^{143}Nd/^{144}Nd$ ratio of 0.512178, which is similar to the one of its footwall host rocks, which is 0.512196.

The obtained elemental composition broadly varies among the different calcite cements and related host rocks (Table 2 and Fig. 12). In the thrust zone affecting the hanging wall, calcite cement Cc1a shows a similar trend to that of the Devonian limestones, both having high Sr, intermediate-high Mg and Fe and low Mn contents (Fig. 12). In the main thrust plane, calcite cement Cc2 has low Mg and Fe and intermediate Mn and Sr contents with respect to the other cements. In the footwall, Cc3 and Cc4 have similar elemental composition, characterized by high Mn, intermediate-high Sr, intermediate-low Fe and low

Mg contents. Finally, calcite cement Cc5 follows a similar trend to that of the Stephano-Permian andesites, both having the highest Fe and Mg and the lowest Sr and Mn contents with respect to the other cements and host rocks.

5 Discussion

5.1 Chronology of the observed structures

The Estamariu thrust, affecting basement rocks in the Axial Pyrenees, resulted from a long-lived tectonic history that lasted from Late Paleozoic (Variscan orogeny) to Neogene times.

The Paleozoic metasedimentary rocks from the Pyrenean basement are broadly affected by multiscale folds and axial plane regional foliation, developed during the main Variscan deformation phase (Bons, 1988; Cochelin et al., 2018; Zwart, 1986). Similar structures, a decametric-scale anticline and pervasive axial plane foliation (S_1), are found in the Devonian sequence located in the thrust hanging wall (Fig. 2B) and therefore, we consider them to be developed during the Variscan compression, contemporaneous with the main activity of the Estamariu thrust. Veins V0 are perpendicular to stylolites e1 and show ambiguous crosscutting relationships between them. Thus, they are interpreted as originated coevally. Both microstructures are concentrated into discontinuous fragments of the Devonian host rocks and are therefore considered inherited microstructures likely developed in Variscan times. However, as pointed above, in the study area the Estamariu thrust affects late- to post-Variscan Stephano-Permian andesites, confirming thus its reactivation during the Alpine orogeny. Accordingly, the structures that are strictly attributed to the Alpine reactivation of the thrust are those structures indicating reverse kinematics or associated with a compressional stress, which are found within the thrust zone deformation, at the contact between Devonian and Stephano-Permian units. Contrarily, the magmatic layering and joints J1 are broadly present in the andesitic footwall, outside the thrust zone, and in other Stephano-Permian basins, and are therefore considered inherited fluidal and cooling structures, respectively. For this reason, the calcite veins V1a and V2 (and related cements Cc1a and Cc2), exclusively occurring within the thrust zone, have been associated with the reactivation of the Estamariu thrust. During this period, and associated with ongoing deformation and progressive shortening, stylolites e2 developed as sutured areas between host rock and veins V1a and between foliation surfaces, coevally with the development of veins V1b, as denoted by their crosscutting relationships and orientations.

Other structures present in the study area, such as veins V3 to V5 and related cements Cc3 to Cc5, are attributed to the Neogene extension. Veins V3 precipitated in the subsidiary thrust zone developed in the footwall of the Estamariu thrust. These veins strike parallel to the thrust zone foliation (S_2) (Fig 7A, B) but are characterized by calcite fibers growing perpendicular to the vein walls and to the foliation surfaces (Fig. 7C), thus evidencing their extensional character. The presence of extensional calcite veins opened along previously formed foliation surfaces in a thrust zone has been reported in other structures in the Pyrenees and has been considered to postdate the thrust activity (Lacroix et al., 2011, 2014). Veins V4 precipitated in subvertical and E-W mesoscale faults affecting the Stephano-Permian andesites (Fig. 8), outside the thrust zone (Fig. 3). The fault orientation and dip and the two striae set generations observed on the fault planes are compatible with the Neogene

285   extensional faults that bound the Cerc basin and postdate the Estamariu thrust (Cabrera et al., 1988; Roca, 1996; Saura, 2004).

Calcite cements Cc3 and Cc4, occluding veins V3 and V4, have a similar geochemical composition (Fig. 9 – 12), supporting that their precipitation occurred during the same tectonic event and associated with a similar fluid regime (i.e., although these cements precipitated in different structures, they are likely contemporaneous). Finally, veins V5 (and related cement Cc5) precipitated locally in shear fractures crosscutting and postdating the thrust-related deformation (Fig. 3, 4 and 8D). These veins

290   strike parallel to the shear bands (Cn) located in the main thrust zone (Fig. 8E), exhibiting normal slip kinematics, postdating the reverse structures and therefore indicating reactivation of the Estamariu thrust during the Neogene extension.

5.2 Fluid system during the Alpine reactivation of the Estamariu thrust

As veins V1a and V2 are consistent with the Alpine reactivation of the Estamariu thrust, the geochemistry of their related calcite cements Cc1a and Cc2 is interpreted to record the fluid system during this tectonic event.

295   Cements Cc1a and Cc2 are characterized by high $^{87}Sr/^{86}Sr$ ratios (from 0.713 to 0.714 for Cc1a and 0.718 for Cc2), significantly more radiogenic than ratios of Phanerozoic seawater (between 0.7070 and 0.7090) (McArthur et al., 2012). This may reflect the incorporation of radiogenic Sr from a fluid derived or interacted with Rb-rich and/or Sr-rich basement rocks such as those underlying the Estamariu thrust. In addition, Cc1a has a narrow range of $\delta^{13}C$, between +0.91 and +2 ‰VPDB, consistent with values of the Devonian marine limestones from the hanging wall (between +1.54 and +2.75 ‰VPDB) and within the range of

300   Devonian marine carbonate values (Veizer et al., 1999). Likewise, the elemental composition of Cc1a follows a similar trend to that of its Devonian host, both having high Mg and Sr and low Mn contents with respect to the other calcite cements (Fig. 12). These geochemical similarities indicate high fluid-rock interaction and buffering of the carbon and elemental composition of the precipitating fluid by the Devonian carbonates (Marshall, 1992). Calcite cement Cc2 has slightly lower $\delta^{13}C$, lower Mg and Sr and higher Mn contents with respect to both Cc1a and the Devonian host. On the other hand, the temperature and the

305     $\delta^{18}O$ composition of the vein-forming fluids, calculated from clumped isotope thermometry of Cc2, range between 50 °C and 100 °C and between -6.4 and -0.3 ‰SMOW, respectively. These values are interpreted as the involvement of meteoric fluids that were probably heated at depth and enriched in radiogenic Sr during their flow and interaction with basement rocks. These fluids flowed preferentially along the thrust zone (Fig. 13A), as evidenced by the exclusive presence of calcite in this area, likely due to the enhanced permeability associated with the thrust discontinuity (McCaig et al., 1995; Trincal et al., 2017). As

310   Cc1a and Cc2 precipitated in the thrust zone during the same tectonic event, they likely precipitated from the same fluids, which progressively increased the extent of fluid-rock interaction from the thrust plane (Cc2) towards the hanging wall (Cc1a), as indicated by the host rock-buffered composition of the latter. Previous studies already reported syntectonic migration of fluids that had interacted at depth with basement rocks before upflowing along thrust zones in other structures from the Pyrenean basement, such as the Gavarnie thrust and the related Pic-de-Port-Vieux thrust (McCaig et al., 1995).

5.3 Fluid system during the Neogene extension

Calcite veins V3 to V5 are attributed to the Neogene extension and the geochemistry of their related calcite cements Cc3 to Cc5 characterize the fluid system during this period.

Cc3 and Cc4 have considerably high $^{87}Sr/^{86}Sr$ ratios (0.714619 and 0.717706, respectively), similar to the ones reported for Cc1a and Cc2 (Fig. 11), indicating interaction with basement rocks. The $\delta^{18}O_{fluid}$ calculated from clumped isotopes, between +4.3 and +12.1 ‰SMOW for Cc3 and between +0.9 and +8.1 ‰SMOW for Cc4, falls within the range of metamorphic and/or formation brines (Taylor, 1987). The $\delta^{18}O$-depleted values of these cements (around -14 ‰VPDB) are due to the high temperatures of the fluids (between 130 °C and 210 °C for Cc3 and between 100 °C and 170 °C for Cc4). Assuming a normal geothermal gradient of 30 °C, these temperatures would have been reached at a minimum depth of 3 – 5 km. However, these veins have never reached such a burial depth, since during the Neogene extension the studied structure acquired its current configuration (Saura, 2004) and was only buried under the Devonian sequence (hanging wall), which has a maximum thickness of several hundred meters (Mey, 1967). This assumption evidences the hydrothermal character of the circulating fluids, which probably migrated rapid enough through normal faults to maintain their high temperatures and to be in thermal disequilibrium with the surrounding rocks. Similarly, the high Mn content of Cc3 and Cc4 (around 7700-8300 and 4000 ppm, respectively), responsible of their bright luminescence (Fig. 7D, 8C), is consistent with hydrothermal waters (Pfeifer et al., 1988; Pomerol, 1983; Pratt et al., 1991). On the other hand, the $\delta^{13}C$-depleted values of these cements are indicative of the influence of organic derived carbon (Cerling, 1984; Vilasi et al., 2006). The most probable source for these low $\delta^{13}C$ values is the Silurian black shales that do not crop out in the study area but acted as the main detachment level during the Variscan compression, and locally during the Alpine compression in the Pyrenean Axial Zone (Mey, 1967). These black shales have significant organic carbon contents (TOC around 2.3%), and around the Gavarnie thrust, they exhibit syntectonic carbonate veins yielding $\delta^{13}C$ values between -2 and -8 ‰VPDB (McCaig et al., 1995). Thus, cements Cc3 and Cc4 precipitated from hydrothermal fluids derived from and/or equilibrated with basement rocks and expelled through newly formed and reactivated fault zones during deformation (Fig. 13B). The hydrothermal character of the fluids involved in this deformation event, and their relative high temperatures (up to 210ºC) could have altered the clumped isotope composition of the previous calcite cement generations (Cc1a and Cc2). Clumped isotopes may be reset by recrystallization and by solid-state isotopic exchange reactions and diffusion within the mineral lattice (Shenton et al., 2015; Stolper and Eiler, 2015). However, in the studied vein samples there is no evidence of calcite recrystallization (for instance, grain coarsening linked to grain boundary migration). Therefore, we conclude that although it is possible, there is little evidence for clumped isotopes of cements Cc1a and Cc2 to have been reset during precipitation of Cc3 and Cc4.

Finally, the isotopic signature of Cc5, ranging between -8.1 and -5.7 ‰VPDB for $\delta^{18}O$ and between -8.2 and -3.8 ‰VPDB for $\delta^{13}C$, falls within the range of meteoric carbonates (Travé et al., 2007; Veizer, 1992). The similar tendency in the elemental composition of this cement and the Stephano-Permian volcanic rocks, both having the highest Mg and Fe and the lowest Mn and Sr contents with respect to the other cements and host rocks, reveals high fluid-rock interaction with the footwall rocks.

The significant water-rock interaction is also demonstrated by the Nd isotopic composition of Cc5 (0.512178), yielding to values of the volcanic host (0.512196). This fact indicates that this cement precipitated from percolation of meteoric fluids, which geochemistry was controlled by the volcanic host rock. Studies focused on infiltration of meteoric fluids and subsequent upflowing along La Tet fault during the Neogene extension have shown that meteoric waters in the area infiltrate at high altitudes, around 2000 m, and low temperatures, around 5°C (Krimissa et al., 1994; Taillefer et al., 2018). Therefore, we suggest that Cc5 probably precipitated during the latest stages of extension, after the fluid regime changed from upward fluid migration to percolation of cold meteoric waters, as also occurred in the Barcelona Plain (Catalan Coastal Ranges) (Cantarero et al., 2014).

In conclusion, the high $^{87}Sr/^{86}Sr$ ratios of the different calcite cements (Cc1a to Cc5) evidence the interaction between the vein-forming fluids and Paleozoic basement rocks with more radiogenic signature. The geochemical evolution of these cement generations also highlights the progressive change in the fluid regime and composition during successive compressional and extensional tectonic events (Fig. 13). The continuous increase in precipitation temperatures and enrichment in $\delta^{18}O_{fluid}$ from calcite cements Cc1a and Cc2 (Alpine) to cements Cc3 and Cc4 (Neogene) is probably linked to higher extent of fluid-rock interaction with basement rocks. By contrast, during the latest stages of extension, the infiltration of meteoric fluids likely indicates a more significant change in the fluid regime, that is, from upward to downward fluid migration (Fig. 13).

5.4 Influence of Paleozoic basement rocks on the $^{87}Sr/^{86}Sr$ ratios of the fluids circulating during deformation

In this section, we assess the influence of basement rocks on the chemistry of fluids circulating during deformation in the Pyrenees. The comparison between previous studies and the new data provided in this contribution evidences that fluids migrating through basement or cover units have a different geochemical signature, which is recorded in the $^{87}Sr/^{86}Sr$ ratios of the vein cements. The high $^{87}Sr/^{86}Sr$ ratios (0.713 to 0.718) of the analyzed cements, originated during successive compressional and extensional tectonic events, indicate that regardless of the origin of the fluids and the tectonic context, basement rocks have a significant influence on the fluid chemistry. Accordingly, cements precipitated from fluids that have circulated through basement rocks have significantly high $^{87}Sr/^{86}Sr$ ratios (> 0.710) (Fig. 11), reflecting the interaction between the vein-forming fluids and rocks with more radiogenic signature. Similar radiogenic $^{87}Sr/^{86}Sr$ ratios have also been attributed to basement-derived fluids in the Glarus nappe (Swiss Alps) (Burkhard et al., 1992). By contrast, vein cements precipitated from fluids that have circulated through the Mesozoic-Cenozoic sedimentary cover in the Pyrenees (i.e., through younger rocks with a different radiogenic signature) have significantly lower $^{87}Sr/^{86}Sr$ ratios (< 0.710). Such lower values may be similar to Phanerozoic seawater values, evidencing interaction between the vein-forming fluids and marine carbonate units, or higher, evidencing interaction with siliciclastic rocks (Cruset et al., 2018; Travé et al., 2007). A previous study, focused on fluid flow along the Gavarnie thrust in the central-western Axial Pyrenees, used this limit value ($^{87}Sr/^{86}Sr = 0.710$) to differentiate between the unaltered limestone protolith and the Cretaceous thrust-related carbonate mylonite affected by fluids carrying radiogenic Sr (McCaig et al., 1995). In addition, (Williams et al., 2015) also attributed $^{87}Sr/^{86}Sr$ ratios > 0.710 to the input of basement-derived fluids in the Rio Grande rift, USA.

5.5 Fluid flow at regional scale: the NE part of the Iberian Peninsula during the Neogene extension

As pointed above, the structural and geochemical data indicate that calcite cements Cc3 and Cc4 (veins V3 and V4, respectively) precipitated from hydrothermal fluids (up to 210 ºC) that interacted at depth with basement rocks before ascending through newly formed and reactivated structures during the Neogene extension. These interpretations are consistent with the presence of several hydrothermal springs (temperatures of 29 ºC to 73 ºC) currently upwelling aligned along La Tet fault and related Neogene deformation in the Pyrenean Axial Zone (Krimissa et al., 1994; Taillefer et al., 2017, 2018). Several studies indicate the origin of these hot water springs as meteoric fluids, infiltrated at high-elevated reliefs, above 2000 m, warmed at great depths by normal geothermal gradients, and migrated upwards along permeability anisotropies related to fault zones (Taillefer et al., 2017, 2018). The $^{87}Sr/^{86}Sr$ ratios of these springs, ranging between 0.715 and 0.730 (Caballero et al., 2012), are within the range of values obtained in this study and also accounts for interaction between circulating fluids and basement lithologies. Studies based on numerical models suggest that La Tet fault and the involved basement rocks are still permeable down to 3 km depth (Taillefer et al., 2017, 2018), although the fault has been dormant since the Mio-Pliocene (Goula et al., 1999). These authors also suggest that the footwall topography, which induces high hydraulic gradients and produces fluid advection, is the major factor controlling the infiltration of meteoric fluids, the circulation depth, and the maximum temperature reached by the migrating fluids (Taillefer et al., 2017).

A similar geological context and fluid regime evolution to that explained above is found in the Barcelona Plain and the Vallès Basin, located in the northeast part of the Catalan Coastal Ranges (CCR) (Fig. 1A). Consequently, the comparison between both geological contexts allows us to give insights into the fluid circulation in extensional basins at regional scale (in the NE part of Iberia). In these locations of the CCR, the main fault system associated with the Neogene extension acted as conduits for hydrothermal fluid circulation at temperatures between 130 and 150 ºC during synkinematic periods (Cantarero et al., 2014; Cardellach et al., 2003), and is also responsible for the present-day circulation of hot water springs up to 70 ºC (Carmona et al., 2000; Fernàndez and Banda, 1990). In both cases, fluids would have been topographically driven from elevated areas to great depths (Cantarero et al., 2014), where they circulated through basement rocks, acquiring high $^{87}Sr/^{86}Sr$ ratios (> 0.712) and high temperatures (Cardellach et al., 2003) before ascending through fault discontinuities. However, in the Penedès basin, which corresponds to the southwestern termination of the Neogene structure in the CCR, basement lithologies do not crop out and the extensional faults only involve Neogene deposits filling the basin and a Mesozoic sedimentary substrate. In this location, the main fault system acted as conduits for several episodes of meteoric fluids percolation during the Neogene extension and evidence of hydrothermal fluid circulation has not been reported in the area (Travé and Calvet, 2001; Travé et al., 1998; Baqués et al., 2012, 2010). This fact agrees with previous studies that highlight that hydrothermal activity, and in particular the occurrence of hot water springs in the Pyrenees and in the CCR, is preferably concentrated in basement rocks, which constitute the elevated footwall of the main extensional fault systems (Taillefer et al., 2017; Carmona et al., 2000).

All these observations indicate an open fluid system in the NE part of the Iberian Peninsula associated with the Neogene extensional deformation. This extensional fault system has acted as a conduit for circulation of hot fluids in Neogene times

and in the present. This fault-controlled fluid flow could have been continuous through time or could be related to intermittent

415 pulses. Fault control on upflowing of hot fluids along fault systems is a common process in different geological settings and has been reported in the Great Basin, USA (Faulds et al., 2010; Nelson et al., 2006), in the Western Turkey (Faulds et al., 2010), in the Southern Canadian Cordillera (Grasby and Hutcheon, 2001) and in the southern Tuscany, Italy (Liotta et al., 2010).

6 Conclusions

420 This study assesses the influence of basement rocks on the fluid chemistry during deformation in the Pyrenees and provides insights into the fluid regime in the NE part of the Iberian Peninsula. Our data indicates that regardless of the fluid origin and the tectonic context, the fluids that have interacted with basement rocks have a higher $^{87}Sr/^{86}Sr$ ratio (> 0.710) than those that have circulated through the sedimentary cover (< 0.710). On the other hand, extensional deformation structures in both the eastern Pyrenees and the northeastern part of the Catalan Coastal Ranges, have acted as conduits for hydrothermal fluid

425 migration in Neogene times and in the present. These fluids likely interacted with basement rocks before ascending through fault zones and related structures.

The studied thrust resulted from a multistage Late Paleozoic (Variscan) to Neogene tectonic evolution. In the study area, it places a Devonian pre-Variscan unit against a Stephano-Permian late to post-Variscan sequence and therefore, the structures present within the thrust zone, affecting both sequences, are attributed to the Alpine compression (Late Cretaceous to

430 Oligocene) and subsequent Neogene extension. During the Alpine compression, the reactivation of the thrust resulted in the transposition of the Variscan regional foliation within the thrust zone and in the formation of a subsidiary thrust zone affecting the andesites in the footwall. Geochemical analyses indicate that meteoric fluids circulated through the thrust during this period at temperatures between 50 and 100 ºC. These fluids progressively increased the extent of fluid-rock interaction from the thrust plane towards the hanging wall, as suggested by the host rock-buffered composition of the calcite in the hanging wall

435 deformation structures. During the Neogene extension, the Estamariu thrust was likely reactivated and normal faults and shear fractures were formed. Geochemical data reveal that basement-derived fluids circulated through these structures at temperatures up to 210 ºC. Finally, during the latest to post stages of extension and uplift of the structure, the fluid regime changed to percolation of meteoric fluids that were buffered by the volcanic host rocks.

Data availability

440 The data used in this study is included within the manuscript and in the supplementary data document.

Author contributions

Conceptualization, DM-L, GA, DC, IC; AT; data curation, DM-L; formal analysis, all authors; funding acquisition, AT; investigation and methodology, all authors; writing-original draft preparation, DM-L; writing-review and editing, all authors.

Competing interest

445   The authors declare that they have no conflict of interest.

Acknowledgments

We acknowledge the constructive comments from Owen Callahan and Brice Lacroix, who helped to improve the quality of the manuscript, as well as the editorial guidance of Randolph Williams. We also thank Josep Maria Casas, from the Universitat de Barcelona, for showing us the location of the studied outcrops. Carbon and oxygen isotopic analyses were carried out at
450   "Centre Científics i Tecnològics" of the Universitat de Barcelona. Strontium and Neodymium analyses were performed at the "CAI de Geocronología y Geoquímica Isotópica" of the Universidad Complutense de Madrid. The Elemental composition was analysed at the Geochemistry Facility of labGEOTOP of Geosciences Barcelona (GEO3BCN-CSIC). Clumped isotope thermometry was carried out at the Imperial College London. This research was carried out within the framework of DGICYT Spanish Project PGC2018-093903-B-C22 (Ministerio de Ciencia, Innovación y Universidades / Agencia Estatal de
455   Investigación / Fondo Europeo de Desarrollo Regional, Unión Europea) and the Grup Consolidat de Recerca "Geologia Sedimentària" (2017-SGR- 824). The PhD research of DM-L is supported by the FPI2016 (BES-2016-077214) Spanish program from MINECO.

References

Arndt, M., Virgo, S., Cox, S. F. and Urai, J. L.: Changes in fluid pathways in a calcite vein mesh (Natih Formation, Oman
460   Mountains): insights from stable isotopes, Geofluids, 14(4), 391–418, doi:10.1111/gfl.12083, 2014.

Banks, D., Da Vies, G., Yardley, B. W., McCaig, A. and Grant, N.: The chemistry of brines from an Alpine thrust system in the Central Pyrenees: An application of fluid inclusion analysis to the study of fluid behaviour in orogenesis, Geochim. Cosmochim. Acta, 55(4), 1021–1030, doi:10.1016/0016-7037(91)90160-7, 1991.

Baques, V., Trave, A., Roca, E., Marin, M. and Cantarero, I.: Geofluid behaviour in successive extensional and compressional
465   events: a case study from the southwestern end of the Valles-Penedes Fault (Catalan Coastal Ranges, NE Spain), Pet. Geosci., 18(1), 17–31, doi:10.1144/1354-079311-017, 2012.

Barker, S. L. L. and Cox, S. F.: Evolution of fluid chemistry and fluid-flow pathways during folding and faulting: an example from Taemas, NSW, Australia, Geol. Soc. London, Spec. Publ., 359(1), 203–227, doi:10.1144/SP359.12, 2011.

Barker, S. L. L., Bennett, V. C., Cox, S. F., Norman, M. D. and Gagan, M. K.: Sm–Nd, Sr, C and O isotope systematics in

470   hydrothermal calcite–fluorite veins: Implications for fluid–rock reaction and geochronology, Chem. Geol., 268(1–2), 58–66, doi:10.1016/j.chemgeo.2009.07.009, 2009.

Beaudoin, N., Bellahsen, N., Lacombe, O., Emmanuel, L. and Pironon, J.: Crustal-scale fluid flow during the tectonic evolution of the Bighorn Basin (Wyoming, USA), Basin Res., 26(3), 403–435, doi:10.1111/bre.12032, 2014.

Beaudoin, N., Huyghe, D., Bellahsen, N., Lacombe, O., Emmanuel, L., Mouthereau, F. and Ouanhnon, L.: Fluid systems and

475   fracture development during syn-depositional fold growth: An example from the Pico del Aguila anticline, Sierras Exteriores, southern Pyrenees, Spain, J. Struct. Geol., 70, 23–38, doi:10.1016/j.jsg.2014.11.003, 2015.

Bickle, M. J., Wickham, S. M., Chapman, H. J. and Taylor, H. P.: A strontium, neodymium and oxygen isotope study of hydrothermal metamorphism and crustal anatexis in the Trois Seigneurs Massif, Pyrenees, France, Contrib. to Mineral. Petrol., 100(4), 399–417, doi:10.1007/BF00371371, 1988.

480   Bons, A.: Intracrystalline deformation and slaty cleavage development in very low-grade slates from the Central Pyrenees, Geol. Ultraiectina, 1988.

Breesch, L., Swennen, R. and Vincent, B.: Fluid flow reconstruction in hanging and footwall carbonates: Compartmentalization by Cenozoic reverse faulting in the Northern Oman Mountains (UAE), Mar. Pet. Geol., 26(1), 113–128, doi:10.1016/j.marpetgeo.2007.10.004, 2009.

485   Burkhard, M., Kerrich, R., Maas, R. and Fyfe, W. S.: Stable and Sr-isotope evidence for fluid advection during thrusting of the glarus nappe (swiss alps), Contrib. to Mineral. Petrol., 112(2–3), 293–311, doi:10.1007/BF00310462, 1992.

Caballero, Y., Gironde, C. and Le Goff, E.: Ressource en eau thermale de la station d'Amélie-les-Bains. Etat des lieux. Rapport BRGM/RP-60618-FR., 2012.

Cabrera, L., Roca, E. and Santanach, P.: Basin formation at the end of a strike-slip fault: the Cerdanya Basin (eastern Pyrenees),

490   J. Geol. Soc. London., 145(2), 261–268, doi:10.1144/gsjgs.145.2.0261, 1988.

Cantarero, I., Travé, A., Alías, G. and Baqués, V.: Polyphasic hydrothermal and meteoric fluid regimes during the growth of a segmented fault involving crystalline and carbonate rocks (Barcelona Plain, NE Spain), Geofluids, 14(1), 20–44, doi:10.1111/gfl.12021, 2014.

Cantarero, I., Alías, G., Cruset, D., Carola, E., Lanari, P. and Travé, A.: Fluid composition changes in crystalline basement

495   rocks from ductile to brittle regimes, Glob. Planet. Change, 171(March), 273–292, doi:10.1016/j.gloplacha.2018.03.002, 2018.

Cardellach, E., Canals, À. and Grandia, F.: Recurrent hydrothermal activity induced by successive extensional episodes: the case of the Berta F–(Pb–Zn) vein system (NE Spain), Ore Geol. Rev., 22(1–2), 133–141, doi:10.1016/S0169-1368(02)00112-9, 2003.

Carmona, J. M., Bitzer, K., López, E. and Bouazza, M.: Isotopic composition and origin of geothermal waters at Caldetes

500   (Maresme-Barcelona), J. Geochemical Explor., 69–70, 441–447, doi:10.1016/S0375-6742(00)00127-8, 2000.

Casas, J. M., Domingo, F., Poblet, J. and Soler, A.: On the role of the Hercynian and Alpine thrusts in the Upper Paleozoic rocks of the Central and Eastern Pyrenees, Geodin. Acta, 3(2), 135–147, doi:10.1080/09853111.1989.11105181, 1989.

Cerling, T. E.: The stable isotopic composition of modern soil carbonate and its relationship to climate, Earth Planet. Sci. Lett., doi:10.1016/0012-821X(84)90089-X, 1984.

505   Choukroune, P.: The Ecors Pyrenean deep seismic profile reflection data and the overall structure of an orogenic belt, Tectonics, doi:10.1029/TC008i001p00023, 1989.

Cochelin, B., Lemirre, B., Denèle, Y., de Saint Blanquat, M., Lahfid, A. and Duchêne, S.: Structural inheritance in the Central Pyrenees: the Variscan to Alpine tectonometamorphic evolution of the Axial Zone, J. Geol. Soc. London., 175(2), 336–351, doi:10.1144/jgs2017-066, 2018.

510   Cox, S. F.: Structural and isotopic constraints on fluid flow regimes and fluid pathways during upper crustal deformation: An example from the Taemas area of the Lachlan Orogen, SE Australia, J. Geophys. Res., 112(B8), B08208, doi:10.1029/2006JB004734, 2007.

Crespo-Blanc, A., Masson, H., Sharp, Z., Cosca, M. and Hunziker, J.: A stable and 40Ar/39Ar isotope study of a major thrust in the Helvetic nappes (Swiss Alps): Evidence for fluid flow and constraints on nappe kinematics, Geol. Soc. Am. Bull.,
515   107(10), 1129–1144, doi:10.1130/0016-7606(1995)107<1129:ASAAAI>2.3.CO;2, 1995.

Crognier, N., Hoareau, G., Aubourg, C., Dubois, M., Lacroix, B., Branellec, M., Callot, J. P. and Vennemann, T.: Syn-orogenic fluid flow in the Jaca basin (south Pyrenean fold and thrust belt) from fracture and vein analyses, Basin Res., 30(2), 187–216, doi:10.1111/bre.12249, 2018.

Cruset, D.: Sequential fluid migration along a fold and thrust belt SE pyrenees from late Cretaceous to Oligocene, PhD thesis,
520   Universitat de Barcelona., 2019.

Cruset, D., Cantarero, I., Travé, A., Vergés, J. and John, C. M.: Crestal graben fluid evolution during growth of the Puig-reig anticline (South Pyrenean fold and thrust belt), J. Geodyn., 101, 30–50, doi:10.1016/j.jog.2016.05.004, 2016.

Cruset, D., Cantarero, I., Vergés, J., John, C. M., Muñoz-López, D. and Travé, A.: Changes in fluid regime in syn-orogenic sediments during the growth of the south Pyrenean fold and thrust belt, Glob. Planet. Change, 171(October 2017), 207–224,
525   doi:10.1016/j.gloplacha.2017.11.001, 2018.

Cruset, D., Cantarero, I., Benedicto, A., John, C. M., Vergés, J., Albert, R., Gerdes, A. and Travé, A.: From hydroplastic to brittle deformation: Controls on fluid flow in fold and thrust belts. Insights from the Lower Pedraforca thrust sheet (SE Pyrenees), Mar. Pet. Geol., 120, 104517, doi:10.1016/j.marpetgeo.2020.104517, 2020a.

Cruset, D., Vergés, J., Albert, R., Gerdes, A., Benedicto, A., Cantarero, I. and Travé, A.: Quantifying deformation processes
530   in the SE Pyrenees using U-Pb dating of fracture-filling calcites, J. Geol. Soc. London., (August), jgs2020-014, doi:10.1144/jgs2020-014, 2020b.

Faulds, J., Coolbaugh, M., Bouchot, V., Moeck, I., Oğuz, K. and Cedex, O.: Characterizing Structural Controls of Geothermal Reservoirs in the Great Basin , USA , and Western Turkey : Developing Successful Exploration Strategies in Extended Terranes, World, C(2010), 25–29, 2010.

535   Faÿ-Gomord, O., Allanic, C., Verbiest, M., Honlet, R., Champenois, F., Bonifacie, M., Chaduteau, C., Wouters, S., Muchez, P., Lasseur, E. and Swennen, R.: Understanding Fluid Flow during Tectonic Reactivation: An Example from the Flamborough

Head Chalk Outcrop (UK), Geofluids, 2018, 1–17, doi:10.1155/2018/9352143, 2018.

Fernàndez, M. and Banda, E.: Geothermal anomalies in the Valles-Penedes Graben Master Fault: Convection through the Horst as a possible mechanism, J. Geophys. Res., 95(B4), 4887, doi:10.1029/JB095iB04p04887, 1990.

540 Fitz-Diaz, E., Hudleston, P., Siebenaller, L., Kirschner, D., Camprubí, A., Tolson, G. and Puig, T. P.: Insights into fluid flow and water-rock interaction during deformation of carbonate sequences in the Mexican fold-thrust belt, J. Struct. Geol., 33(8), 1237–1253, doi:10.1016/j.jsg.2011.05.009, 2011.

Foden, J.: Sr-isotopic evidence for Late Neoproterozoic rifting in the Adelaide Geosyncline at 586 Ma: implications for a Cu ore forming fluid flux, Precambrian Res., 106(3–4), 291–308, doi:10.1016/S0301-9268(00)00132-7, 2001.

545 Fontana, S., Nader, F. H., Morad, S., Ceriani, A., Al-Aasm, I. S., Daniel, J. M. and Mengus, J. M.: Fluid-rock interactions associated with regional tectonics and basin evolution, Sedimentology, 61(3), 660–690, doi:10.1111/sed.12073, 2014.

García-Sansegundo, J., Poblet, J., Alonso, J. L. and Clariana, P.: Hinterland-foreland zonation of the Variscan orogen in the Central Pyrenees: comparison with the northern part of the Iberian Variscan Massif, Geol. Soc. London, Spec. Publ., 349(1), 169–184, doi:10.1144/SP349.9, 2011.

550 Gasparrini, M., Ruggieri, G. and Brogi, A.: Diagenesis versus hydrothermalism and fluid-rock interaction within the Tuscan Nappe of the Monte Amiata CO_2-rich geothermal area (Italy), Geofluids, 13(2), 159–179, doi:10.1111/gfl.12025, 2013.

Gomez-Rivas, E., Bons, P. D., Koehn, D., Urai, J. L., Arndt, M., Virgo, S., Laurich, B., Zeeb, C., Stark, L. and Blum, P.: The Jabal Akhdar dome in the Oman Mountains: Evolution of a dynamic fracture system, Am. J. Sci., 314(7), 1104–1139, doi:10.2475/07.2014.02, 2014.

555 Goula, X., Olivera, C., Fleta, J., Grellet, B., Lindo, R., Rivera, L. A., Cisternas, A. and Carbon, D.: Present and recent stress regime in the eastern part of the Pyrenees, Tectonophysics, doi:10.1016/S0040-1951(99)00120-1, 1999.

Grant, N. T., Banks, D. A., McCaig, A. M. and Yardley, B. W. D.: Chemistry, source, and behavior of fluids involved in alpine thrusting of the Central Pyrenees, J. Geophys. Res., 95(B6), 9123, doi:10.1029/JB095iB06p09123, 1990.

Grasby, S. E. and Hutcheon, I.: Controls on the distribution of thermal springs in the southern Canadian Cordillera, Can. J. 560 Earth Sci., 38(3), 427–440, doi:10.1139/cjes-38-3-427, 2001.

Hartevelt, J. J. A.: Geology of the Upper Segre and Valira Valleys, Central Pyrenees, Andorra, Spain, Geological Institute, Leiden University, Leiden, 1970.

Henderson, I. H. C. and McCaig, A. M.: Fluid pressure and salinity variations in shear zone-related veins, central Pyrenees, France: Implications for the fault-valve model, Tectonophysics, 262(1–4), 321–348, doi:10.1016/0040-1951(96)00018-2, 565 1996.

Kluge, T., John, C. M., Jourdan, A.-L., Davis, S. and Crawshaw, J.: Laboratory calibration of the calcium carbonate clumped isotope thermometer in the 25–250 °C temperature range, Geochim. Cosmochim. Acta, 157, 213–227, doi:10.1016/j.gca.2015.02.028, 2015.

Krimissa, M., Chery, L., Fouillac, C. and Michelot, J. L.: Origin and Recharge Altitude of the Thermo-Mineral Waters of the 570 Eastern Pyrenees, Isot. Isot. Environ. Heal. Stud., 30(4), 317–331, doi:10.1080/00211919408046747, 1994.

Lacroix, B., Buatier, M., Labaume, P., Travé, A., Dubois, M., Charpentier, D., Ventalon, S. and Convert-Gaubier, D.: Microtectonic and geochemical characterization of thrusting in a foreland basin: Example of the South-Pyrenean orogenic wedge (Spain), J. Struct. Geol., 33(9), 1359–1377, doi:10.1016/j.jsg.2011.06.006, 2011.

575   Lacroix, B., Travé, A., Buatier, M., Labaume, P., Vennemann, T. and Dubois, M.: Syntectonic fluid-flow along thrust faults: Example of the South-Pyrenean fold-and-thrust belt, Mar. Pet. Geol., 49, 84–98, doi:10.1016/j.marpetgeo.2013.09.005, 2014.

Lacroix, B., Baumgartner, L. P., Bouvier, A.-S., Kempton, P. D. and Vennemann, T.: Multi fluid-flow record during episodic mode I opening: A microstructural and SIMS study (Cotiella Thrust Fault, Pyrenees), Earth Planet. Sci. Lett., 503, 37–46, doi:10.1016/j.epsl.2018.09.016, 2018.

Lago, M., Arranz, E., Pocoví, A., Galé, C. and Gil-Imaz, A.: Permian magmatism and basin dynamics in the southern Pyrenees:

580   a record of the transition from late Variscan transtension to early Alpine extension, Geol. Soc. London, Spec. Publ., 223(1), 439–464, doi:10.1144/GSL.SP.2004.223.01.19, 2004.

Liotta, D., Ruggieri, G., Brogi, A., Fulignati, P., Dini, A. and Nardini, I.: Migration of geothermal fluids in extensional terrains: the ore deposits of the Boccheggiano-Montieri area (southern Tuscany, Italy), Int. J. Earth Sci., 99(3), 623–644, doi:10.1007/s00531-008-0411-3, 2010.

585   Marshall, J. D.: Climatic and oceanographic isotopic signals from the carbonate rock record and their preservation, Geol. Mag., doi:10.1017/S0016756800008244, 1992.

Martí, J.: Caldera-like structures related to Permo-Carboniferous volcanism of the Catalan Pyrenees (NE Spain), J. Volcanol. Geotherm. Res., 45(3–4), 173–186, doi:10.1016/0377-0273(91)90057-7, 1991.

Martí, J.: Genesis of crystal-rich volcaniclastic facies in the Permian red beds of the Central Pyrenees (NE Spain), Sediment.

590   Geol., 106(1–2), 1–19, doi:10.1016/0037-0738(95)00143-3, 1996.

Martín-Martín, J. D., Travé, A., Gomez-Rivas, E., Salas, R., Sizun, J. P., Vergés, J., Corbella, M., Stafford, S. L. and Alfonso, P.: Fault-controlled and stratabound dolostones in the Late Aptian-earliest Albian Benassal Formation (Maestrat Basin, E Spain): Petrology and geochemistry constrains, Mar. Pet. Geol., 65, doi:10.1016/j.marpetgeo.2015.03.019, 2015.

Martinez Casas, L. F., Travé, A., Cruset, D. and Muñoz-López, D.: The Montagut Fault System: Geometry and Fluid Flow

595   Analysis (Southern Pyrennes, Spain), in Petrogenesis and Exploration of the Earth's Interior. Proceedings of the 1st Springer Conference of the Arabian Journal of Geosciences (CAJG-1), Tunisia 2018, pp. 211–214., 2019.

McArthur, J. M., Howarth, R. J. and Shields, G. A.: Strontium Isotope Stratigraphy, in The Geologic Time Scale, vol. 1–2, pp. 127–144, Elsevier., 2012.

McCaig, A., Tritlla, J. and Banks, D.: Fluid mixing and recycling during Pyrenean thrusting: evidence from fluid inclusion

600   halogen ratios, Geochim. Cosmochim. Acta, 64(19), 3395–3412, doi:10.1016/S0016-7037(00)00437-3, 2000a.

McCaig, A. M., Wayne, D. M., Marshall, J. D., Banks, D. and Henderson, I.: Isotopic and fluid inclusion studies of fluid movement along the Gavarnie Thrust, central Pyrenees; reaction fronts in carbonate mylonites, Am. J. Sci., 295(3), 309–343, doi:10.2475/ajs.295.3.309, 1995.

McCaig, A. M., Wayne, D. M. and Rosenbaum, J. M.: Fluid expulsion and dilatancy pumping during thrusting in the Pyrenees:

605 Pb and Sr isotope evidence, Geol. Soc. Am. Bull., 112(8), 1199–1208, doi:10.1130/0016-7606(2000)112<1199:FEADPD>2.0.CO;2, 2000b.

Mey, P. H. W.: The geology of the upper Ribagorzana and Baliera Valleys, Central Pyrenees, Spain, Leidse Geol. Meded., 41, 153–220, 1967.

Mey, P. H. W., Nagtegaal, P. J. C., Roberti, K. J. and Hartevelt, J. J. A.: Lithostratigraphic subdivision of Post-Hercynian

610 deposits in the South-Central Pyrenees, Spain, Leidse Geol. Meded., 41(1), 221–228, 1968.

Mouthereau, F., Filleaudeau, P. Y., Vacherat, A., Pik, R., Lacombe, O., Fellin, M. G., Castelltort, S., Christophoul, F. and Masini, E.: Placing limits to shortening evolution in the Pyrenees: Role of margin architecture and implications for the Iberia/Europe convergence, Tectonics, 33(12), 2283–2314, doi:10.1002/2014TC003663, 2014.

Mozafari, M., Swennen, R., Balsamo, F., El Desouky, H., Storti, F. and Taberner, C.: Fault-controlled dolomitization in the

615 Montagna dei Fiori Anticline (Central Apennines, Italy): record of a dominantly pre-orogenic fluid migration, Solid Earth, 10(4), 1355–1383, doi:10.5194/se-10-1355-2019, 2019.

Muñoz-López, D., Cruset, D., Cantarero, I., Benedicto, A., John, C. M. and Travé, A.: Fluid Dynamics in a Thrust Fault Inferred from Petrology and Geochemistry of Calcite Veins: An Example from the Southern Pyrenees, Geofluids, 2020, 8815729, doi:10.1155/2020/8815729, 2020.

620 Muñoz, J. A.: Evolution of a continental collision belt: ECORS-Pyrenees crustal balanced cross-section, in Thrust Tectonics, pp. 235–246, Springer Netherlands, Dordrecht., 1992.

Muñoz, J. A.: Fault-related folds in the southern Pyrenees, Am. Assoc. Pet. Geol. Bull., 101(04), 579–587, doi:10.1306/011817DIG17037, 2017.

Muñoz, J. A., Martinez, A. and Verges, J.: Thrust sequences in the eastern Spanish Pyrenees, J. Struct. Geol., 8, 399–405,

625 1986.

Nardini, N., Muñoz-López, D., Cruset, D., Cantarero, I., Martín-Martín, J., Benedicto, A., Gomez-Rivas, E., John, C. and Travé, A.: From Early Contraction to Post-Folding Fluid Evolution in the Frontal Part of the Bóixols Thrust Sheet (Southern Pyrenees) as Revealed by the Texture and Geochemistry of Calcite Cements, Minerals, 9(2), 117, doi:10.3390/min9020117, 2019.

630 Nelson, S. T., Mayo, A. L., Gilfillan, S., Dutson, S. J., Harris, R. A., Shipton, Z. K. and Tingey, D. G.: Enhanced fracture permeability and accompanying fluid flow in the footwall of a normal fault: The Hurricane fault at Pah Tempe hot springs, Washington County, Utah, Geol. Soc. Am. Bull., preprint(2008), 1, doi:10.1130/B26285.1, 2006.

Pfeifer, H.-R., Oberhänsli, H. and Epprecht, W.: Geochemical evidence for a synsedimentary hydrothermal origin of Jurassic iron-manganese deposits at Gonzen (Sargans, Helvetic Alps, Switzerland), Mar. Geol., 84(3–4), 257–272, doi:10.1016/0025-

635 3227(88)90105-3, 1988.

Piessens, K., Muchez, P., Dewaele, S., Boyce, A., De Vos, W., Sintubin, M., Debacker, T. N., Burke, E. A. J. and Viaene, W.: Fluid flow, alteration and polysulphide mineralisation associated with a low-angle reverse shear zone in the Lower Palaeozoic of the Anglo-Brabant fold belt, Belgium, Tectonophysics, doi:10.1016/S0040-1951(01)00250-5, 2002.

Poblet, J.: Estructura herciniana i alpina del vessant sud de la zona axial del Pirineu centra, Universitat de barcelona., 1991.

640   Pomerol, B.: Geochemistry of the late Cenomanian-early Turonian chalks of the Paris Basin: Manganese and carbon isotopes in carbonates as paleooceanographic indicators, Cretac. Res., 4(1), 85–93, doi:10.1016/0195-6671(83)90025-3, 1983.

Pratt, L. M., Force, E. R. and Pomerol, B.: Coupled manganese and carbon-isotopic events in marine carbonates at the Cenomanian-Turonian boundary, J. Sediment. Petrol., doi:10.1306/D4267717-2B26-11D7-8648000102C1865D, 1991.

Roca, E.: The Neogene Cerdanya and Seu d'Urgell intramontane basins (Eastern Pyrenees), in Tertiary basins of Spain, edited

645   by P. F. Friend and C. J. Dabrio, pp. 114–119, Cambridge University Press, Cambridge., 1996.

Roca, E. and Guimerà, J.: The Neogene structure of the eastern Iberian margin: Structural constraints on the crustal evolution of the Valencia trough (western Mediterranean), Tectonophysics, 203(1–4), 203–218, doi:10.1016/0040-1951(92)90224-T, 1992.

Roure, F., Choukroune, P., Berastegui, X., Munoz, J. a., Villien, A., Matheron, P., Bareyt, M., Seguret, M., Camara, P. and

650   Deramond, J.: Ecors deep seismic data and balanced cross sections: Geometric constraints on the evolution of the Pyrenees, Tectonics, 8(1), 41–50, doi:10.1029/TC008i001p00041, 1989.

Rowland, J. V. and Sibson, R. H.: Structural controls on hydrothermal flow in a segmented rift system, Taupo Volcanic Zone, New Zealand, Geofluids, 4(4), 259–283, doi:10.1111/j.1468-8123.2004.00091.x, 2004.

Rye, D. M. and Bradbury, H. J.: Fluid flow in the crust; an example from a Pyrenean thrust ramp, Am. J. Sci., 288(3), 197–

655   235, doi:10.2475/ajs.288.3.197, 1988.

Saura, E.: Analisi estructural de la Zona de les Nogures (Pirineus Centrals), PhD thesis, Universitat de Barcelona., 2004.

Saura, E. and Teixell, A.: Inversion of small basins: effects on structural variations at the leading edge of the Axial Zone antiformal stack (Southern Pyrenees, Spain), J. Struct. Geol., 28(11), 1909–1920, doi:10.1016/j.jsg.2006.06.005, 2006.

Shenton, B. J., Grossman, E. L., Passey, B. H., Henkes, G. A., Becker, T. P., Laya, J. C., Perez-Huerta, A., Becker, S. P. and

660   Lawson, M.: Clumped isotope thermometry in deeply buried sedimentary carbonates: The effects of bond reordering and recrystallization, Geol. Soc. Am. Bull., 127(7–8), B31169.1, doi:10.1130/B31169.1, 2015.

Sibson, R. H.: Crustal stress, faulting and fluid flow, Geol. Soc. London, Spec. Publ., 78(1), 69–84, doi:10.1144/GSL.SP.1994.078.01.07, 1994.

Sibson, R. H.: Selective fault reactivation during basin inversion: potential for fluid redistribution through fault-valve action,

665   Geol. Soc. London, Spec. Publ., 88(1), 3–19, doi:10.1144/GSL.SP.1995.088.01.02, 1995.

Sibuet, J. C., Srivastava, S. P. and Spakman, W.: Pyrenean orogeny and plate kinematics, J. Geophys. Res. B Solid Earth, 109(8), 1–18, doi:10.1029/2003JB002514, 2004.

Srivastava, S. P., Schouten, H., Roest, W. R., Klitgord, K. D., Kovacs, L. C., Verhoef, J. and Macnab, R.: Iberian plate kinematics: A jumping plate boundary between Eurasia and Africa, Nature, doi:10.1038/344756a0, 1990.

670   Stolper, D. A. and Eiler, J. M.: The kinetics of solid-state isotope-exchange reactions for clumped isotopes: A study of inorganic calcites and apatites from natural and experimental samples, Am. J. Sci., 315(5), 363–411, doi:10.2475/05.2015.01, 2015.

Suchy, V., Heijlen, W., Sykorova, I., Muchez, P., Dobes, P., Hladikova, J., Jackova, I., Safanda, J. and Zeman, A.: Geochemical study of calcite veins in the Silurian and Devonian of the Barrandian Basin (Czech Republic): evidence for

675 widespread post-Variscan fluid flow in the central part of the Bohemian Massif, Sediment. Geol., 131(3–4), 201–219, doi:10.1016/S0037-0738(99)00136-0, 2000.

Taillefer, A., Soliva, R., Guillou-Frottier, L., Le Goff, E., Martin, G. and Seranne, M.: Fault-Related Controls on Upward Hydrothermal Flow: An Integrated Geological Study of the Têt Fault System, Eastern Pyrénées (France), Geofluids, 2017, 1–19, doi:10.1155/2017/8190109, 2017.

680 Taillefer, A., Guillou-Frottier, L., Soliva, R., Magri, F., Lopez, S., Courrioux, G., Millot, R., Ladouche, B. and Le Goff, E.: Topographic and Faults Control of Hydrothermal Circulation Along Dormant Faults in an Orogen, Geochemistry, Geophys. Geosystems, 19(12), 4972–4995, doi:10.1029/2018GC007965, 2018.

Taylor, B. D.: Stable isotope geochemistry of ore-forming fluids, in Short Course Handbook., 1987.

Travé, A., Labaume, P., Calvet, F. and Soler, A.: Sediment dewatering and pore fluid migration along thrust faults in a foreland

685 basin inferred from isotopic and elemental geochemical analyses (Eocene southern Pyrenees, Spain), Tectonophysics, 282(1–4), 375–398, doi:10.1016/S0040-1951(97)00225-4, 1997.

Travé, A., Labaume, P., Calvet, F., Soler, A., Tritlla, J., Buatier, M., Potdevin, J.-L., Séguret, M., Raynaud, S. and Briqueu, L.: Fluid migration during Eocene thrust emplacement in the south Pyrenean foreland basin (Spain): an integrated structural, mineralogical and geochemical approach, Geol. Soc. London, Spec. Publ., 134(1), 163–188,

690 doi:10.1144/GSL.SP.1998.134.01.08, 1998.

Travé, A., Calvet, F., Sans, M., Vergés, J. and Thirlwall, M.: Fluid history related to the Alpine compression at the margin of the south-Pyrenean Foreland basin: the El Guix anticline, Tectonophysics, 321(1), 73–102, doi:10.1016/S0040-1951(00)00090-1, 2000.

Travé, A., Labaume, P. and Vergés, J.: Fluid Systems in Foreland Fold-and-Thrust Belts: An Overview from the Southern

695 Pyrenees, in Thrust Belts and Foreland Basins, edited by O. Lacombe, F. Roure, J. Lavé, and J. Vergés, pp. 93–115, Springer Berlin Heidelberg, Berlin, Heidelberg., 2007.

Travé, A., Roca, E., Playà, E., Parcerisa, D., Gómez-Gras, D. and Martín-Martín, J. D.: Migration of Mn-rich fluids through normal faults and fine-grained terrigenous sediments during early development of the Neogene Vallès-Penedès half-graben (NE Spain), Geofluids, 9(4), 303–320, doi:10.1111/j.1468-8123.2009.00258.x, 2009.

700 Trincal, V., Buatier, M., Charpentier, D., Lacroix, B., Lanari, P., Labaume, P., Lahfid, A. and Vennemann, T.: Fluid–rock interactions related to metamorphic reducing fluid flow in meta-sediments: example of the Pic-de-Port-Vieux thrust (Pyrenees, Spain), Contrib. to Mineral. Petrol., 172(9), 78, doi:10.1007/s00410-017-1394-5, 2017.

Veizer, J.: Depositional and diagenetic history of limestones: Stable and radiogenic isotopes, in Isotopic Signatures and Sedimentary Records, pp. 13–48, Springer-Verlag, Berlin/Heidelberg., 1992.

705 Veizer, J., Ala, D., Azmy, K., Bruckschen, P., Buhl, D., Bruhn, F., Carden, G. A. F., Diener, A., Ebneth, S., Godderis, Y., Jasper, T., Korte, C., Pawellek, F., Podlaha, O. G. and Strauss, H.: 87Sr/86Sr, δ13C and δ18O evolution of Phanerozoic

seawater, Chem. Geol., 161(1–3), 59–88, doi:10.1016/S0009-2541(99)00081-9, 1999.

Vergés, J.: Estudi geològic del vessant Sud del Pirineu Oriental i Central: Evolució cinemàtica en 3D. PhD thesis, University of barcelona, Barcelona., 1993.

710   Vergés, J. and Fernàndez, M.: Tethys–Atlantic interaction along the Iberia–Africa plate boundary: The Betic–Rif orogenic system, Tectonophysics, 579, 144–172, doi:10.1016/j.tecto.2012.08.032, 2012.

Vergés, J. and Muñoz, J. A.: Thrust sequences in the southern central Pyrenees, Bull. French Geol. Soc., 2, 265–271, 1990.

Vergés, J., Fernàndez, M. and Martìnez, A.: The Pyrenean orogen: pre-, syn-, and post-collisional evolution, J. Virtual Explor., 08(January 2002), doi:10.3809/jvirtex.2002.00058, 2002.

715   Vilasi, N., Swennen, R. and Roure, F.: Diagenesis and fracturing of Paleocene-Eocene carbonate turbidite systems in the Ionian Basin: The example of the Kelçyra area (Albania), J. Geochemical Explor., 89(1-3 SPEC. ISS.), 409–413, doi:10.1016/j.gexplo.2005.11.018, 2006.

Vinet, L. and Zhedanov, A.: A "missing" family of classical orthogonal polynomials, edited by Intergovernmental Panel on Climate Change, Clim. Chang. 2013 - Phys. Sci. Basis, 1–30, doi:10.1088/1751-8113/44/8/085201, 2010.

720   Voicu, G., Bardoux, M., Stevenson, R. and Jébrak, M.: Nd and Sr isotope study of hydrothermal scheelite and host rocks at Omai, Guiana Shield: implications for ore fluid source and flow path during the formation of orogenic gold deposits, Miner. Depos., 35(4), 302–314, doi:10.1007/s001260050243, 2000.

Warren, J., Morley, C. K., Charoentitirat, T., Cartwright, I., Ampaiwan, P., Khositchaisri, P., Mirzaloo, M. and Yingyuen, J.: Structural and fluid evolution of Saraburi Group sedimentary carbonates, central Thailand: A tectonically driven fluid system,
725   Mar. Pet. Geol., 55, 100–121, doi:10.1016/j.marpetgeo.2013.12.019, 2014.

Wayne, D. M. and McCaig, A. M.: Dating fluid flow in shear zones: Rb-Sr and U-Pb studies of syntectonic veins in the Néouvielle Massif, Pyrenees, Geol. Soc. London, Spec. Publ., 144(1), 129–135, doi:10.1144/GSL.SP.1998.144.01.09, 1998.

Williams, R. T., Goodwin, L. B., Mozley, P. S., Beard, B. L. and Johnson, C. M.: Tectonic controls on fault zone flow pathways in the rio grande rift, New Mexico, USA, Geology, 43(8), 723–726, doi:10.1130/G36799.1, 2015.

730   Ziegler, P. A.: Evolution of te Arctic-North Atlantic andthe Western Tethys, in AAPG Memoir Volume 43: Evolution of the Arctic-North Atlantic and the Western Tethys., 1988.

Zwart, H. J.: The variscan geology of the Pyrenees, Tectonophysics, 129(1–4), 9–27, doi:10.1016/0040-1951(86)90243-X, 1986.

735

740

Table 1. $\delta^{18}O$, $\delta^{13}C$, $^{87}Sr/^{86}Sr$ and $^{143}Nd/^{144}Nd$ ratios of the calcite cements and related host rocks. The calculated precipitation temperature and the $\delta^{18}O_{fluid}$ of the parent fluids are also indicated. NR indicates analyzed samples in which no result was obtained.
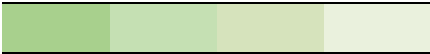
Sample	Vein	Cement	$\delta^{18}O$ ‰VPDB	$\delta^{13}C$ ‰VPDB	$^{87}Sr/^{86}Sr$	$^{143}Nd/^{144}Nd$	Δ_{47}	T (°C)	$\delta^{18}O_{fluid}$ ‰SMOW
C9	V1a	Cc1a	-11.2	+0.91					
C8B	V1a	Cc1a	-10.7	+2					
C8A.I	V1a	Cc1a	-10.4	+2					
C8A.II	V1a	Cc1a	-10.96	+1.3	0.713018	NR			
C8A.III	V1a	Cc1a	-10.9	+1.2					
C7.I	V1a	Cc1a	-10.9	+2.1					
C7.II	V1a	Cc1a	-10.8	+0.8					
C7.III	V1a	Cc1a	-10.4	+1.96					
C4B	V1a	Cc1a	-10.3	+1.9	0.714092	NR			
C3A.I	V1a	Cc1a	-11.2	+1.9					
C3A.II	V1a	Cc1a	-11.3	+1.7					
C3A.III	V1a	Cc1a	-10.5	+1.98					
C15.I	V2	Cc2	-14.9	-1.2	0.718294	NR	0.567	50 to 100	-0.3 to -6.4
C15.II	V2	Cc2	-13.3	+0.5					
C15.III	V2	Cc2	-12.91	+1.54					
C13	V3	Cc3	-13.8	-7.1	0.714619	NR	0.445	130 to 210	+4.3 to +12.1
C12.II	V3	Cc3	-14.3	-7.3					
C10	V3	Cc3	-14.2	-9.3					
C11A	V3	Cc3	-14.2	-8.7					
C13.II	V3	Cc3	-13.6	-7.2					
C14.I	V3	Cc3	-13.4	-6.9					
C14.II	V3	Cc3	-13.7	-7.4					
C16A	V3	Cc3	-13.8	-7.2					
C16B	V3	Cc3	-14	-7					
C16C	V3	Cc3	-14.1	-6.9					
C18.I	V4	Cc4	-13.4	-7.2	0.717706	NR	0.48	100 to 170	+0.9 to +8.1
C18.II	V4	Cc4	-13.8	-7.4					
C12.I	V5	Cc5	-8.1	-7.8	0.716923	0.512178			
C6.I	V5	Cc5	-6.7	-8.2					
C6.II	V5	Cc5	-7.4	-7.4					
C11B	V5	Cc5	-5.7	-3.8					
C3A.HR	Devonian		-9.5	+2.4	0.710663	NR			
C17.HR	carbonates		-10.5	+1.5					
C4.HR			-8.4	+2.7					
C11.HR	Andesites			-	0.743983	0.512196			

745

Table 2: Elemental composition (Ca, Mg, Fe, Mn, Sr) of the calcite cements Cc1a to Cc5 and host rocks from the hanging wall (HW) and footwall (FW). The qualitative scale in greens indicates different contents (for each element, the darkest green points to the highest concentration and vice versa).

Sample	Ca ppm	Mg ppm	Fe ppm	Mn ppm	Sr ppm
Cc1a	391618	1335.9	5603.5	1243.7	543.7
Cc1a	349063	1548.6	4121.3	781.6	460.2
Cc1a	351134	1231.8	5205.4	810.3	545.5
Cc1a	337588	1126.6	3914.9	680.7	704.0
Cc2	328169	501.2	1061.4	3629.3	248.5
Cc3	364995	331.9	1647.8	8277.9	122.3
Cc3	333123	909.5	5545.9	7695.5	424.9
Cc4	333563	624.4	3814.9	4034.6	72.2
Cc5	233784	2260.0	8656.6	161.4	72.1
Cc5	281741	1626.2	4078.0	138.8	25.3
HW	320038	2752.6	6289.0	621.1	449.4
FW	4234	12830.5	43107.1	466.6	18.6

Higher content   Lower content
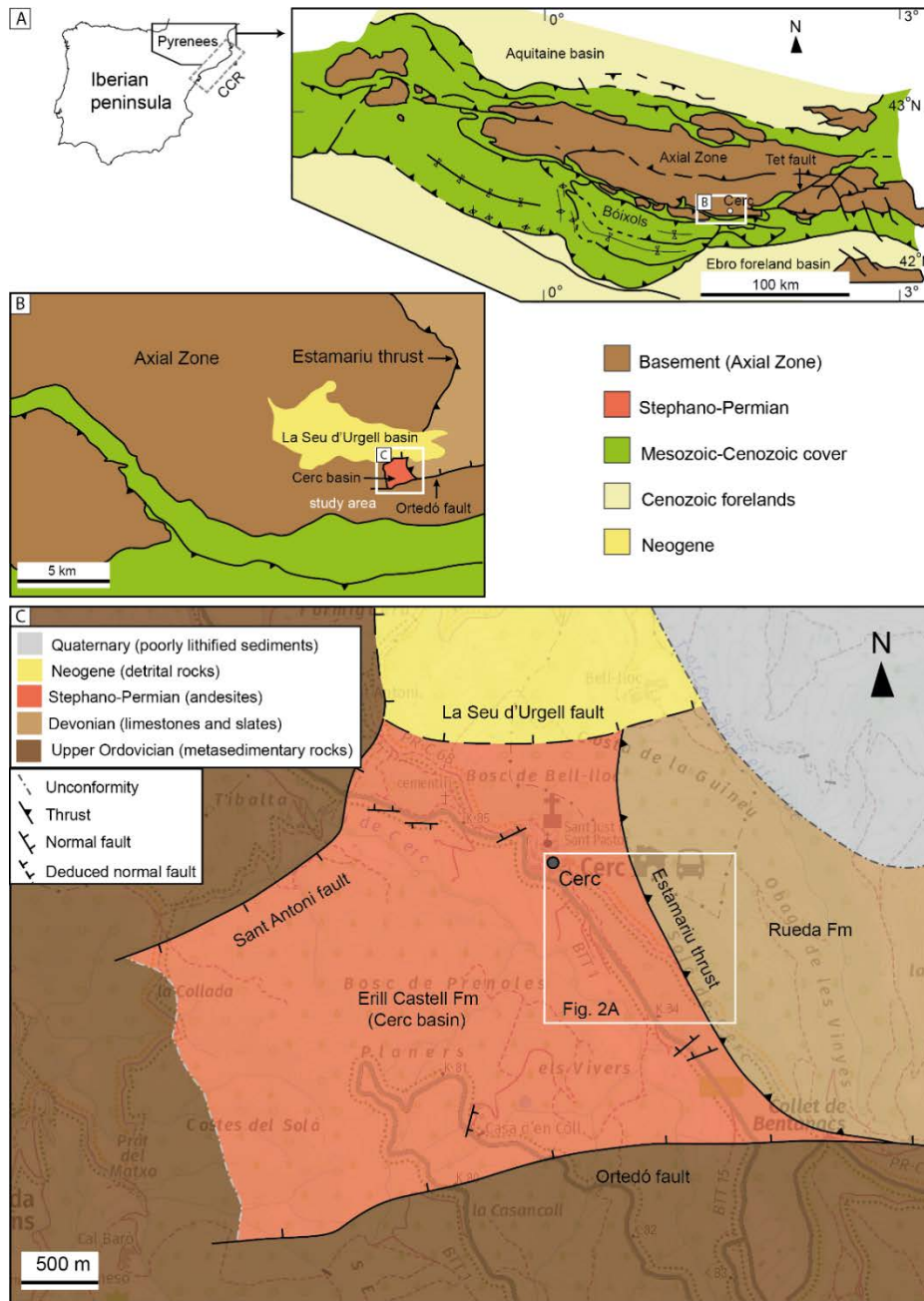
Figure 1: (A) Simplified geological map of the Pyrenees modified from (Muñoz, 2017) and its location in the Iberian Peninsula (location of the Catalan Coastal Range, CCR, is also shown). **(B)** Detail of the study area located within the Pyrenean Axial zone. **(C)** Geological map of the Cerc basin (using data from Saura (2004) and our own data) with the Estamariu thrust located in its eastern termination and the Neogene extensional faults in the northern and southern limits. The white square indicates the location of the main outcrop (Fig. 2A).

760
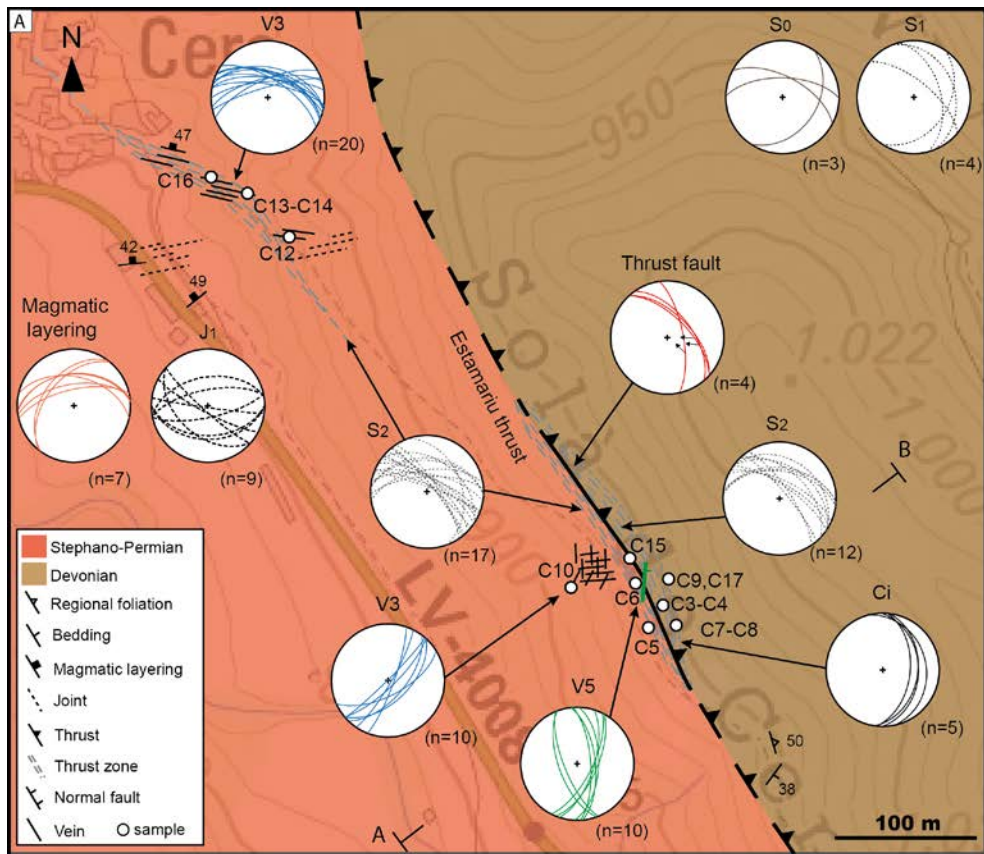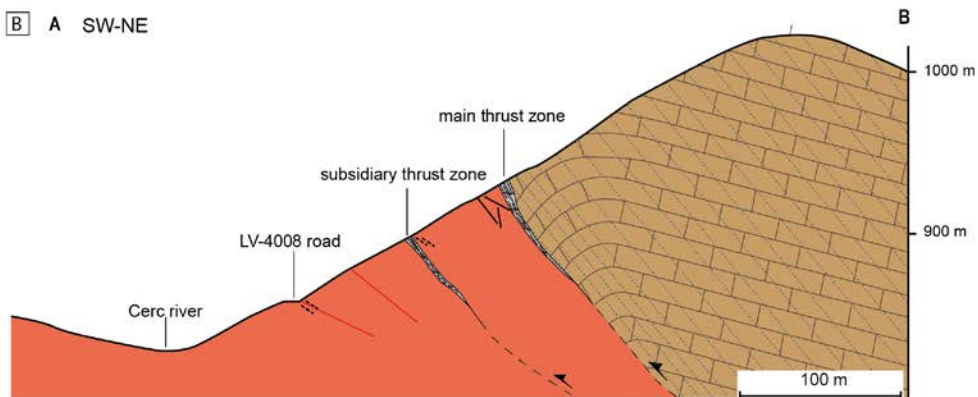
Figure 2: (A) Geological map and **(B)** cross-section of the Estamariu thrust, which juxtaposes a Devonian unit against a Stephano-Permian sequence (H=V, no vertical exaggeration). Lower-hemisphere equal-area stereoplots of the Devonian bedding (S_0), regional foliation (S_1), thrust zone foliation affecting the hanging wall and footwall (S_2), magmatic layering and the different faults and veins observed in the study area are also included. Location in Fig. 1B.

765
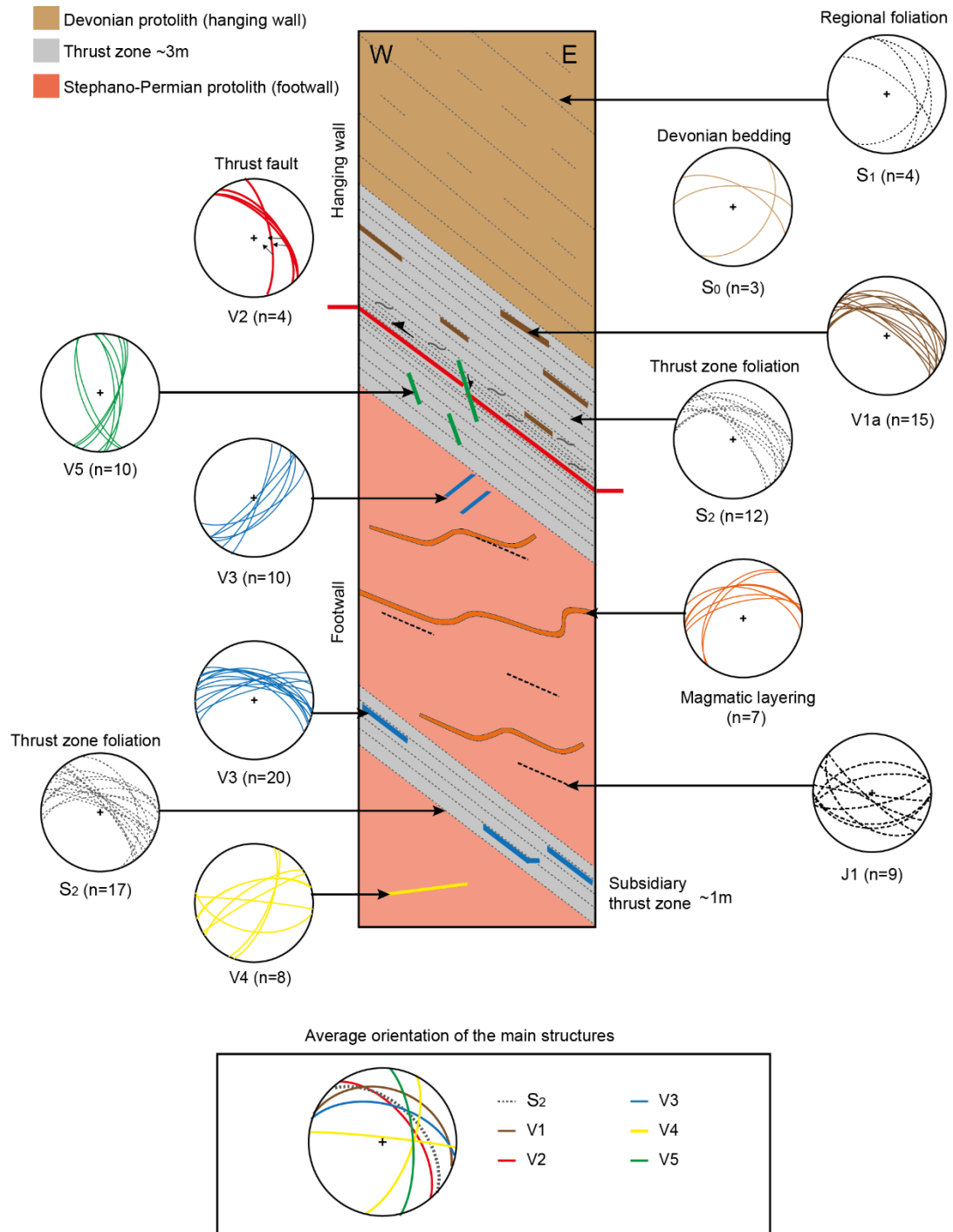
Figure 3: Sketch showing the spatial distribution of mesoscale structures within the main outcrop and lower-hemisphere equal-area stereoplots of the different mesostructures. The average orientation of the main structures is also provided.
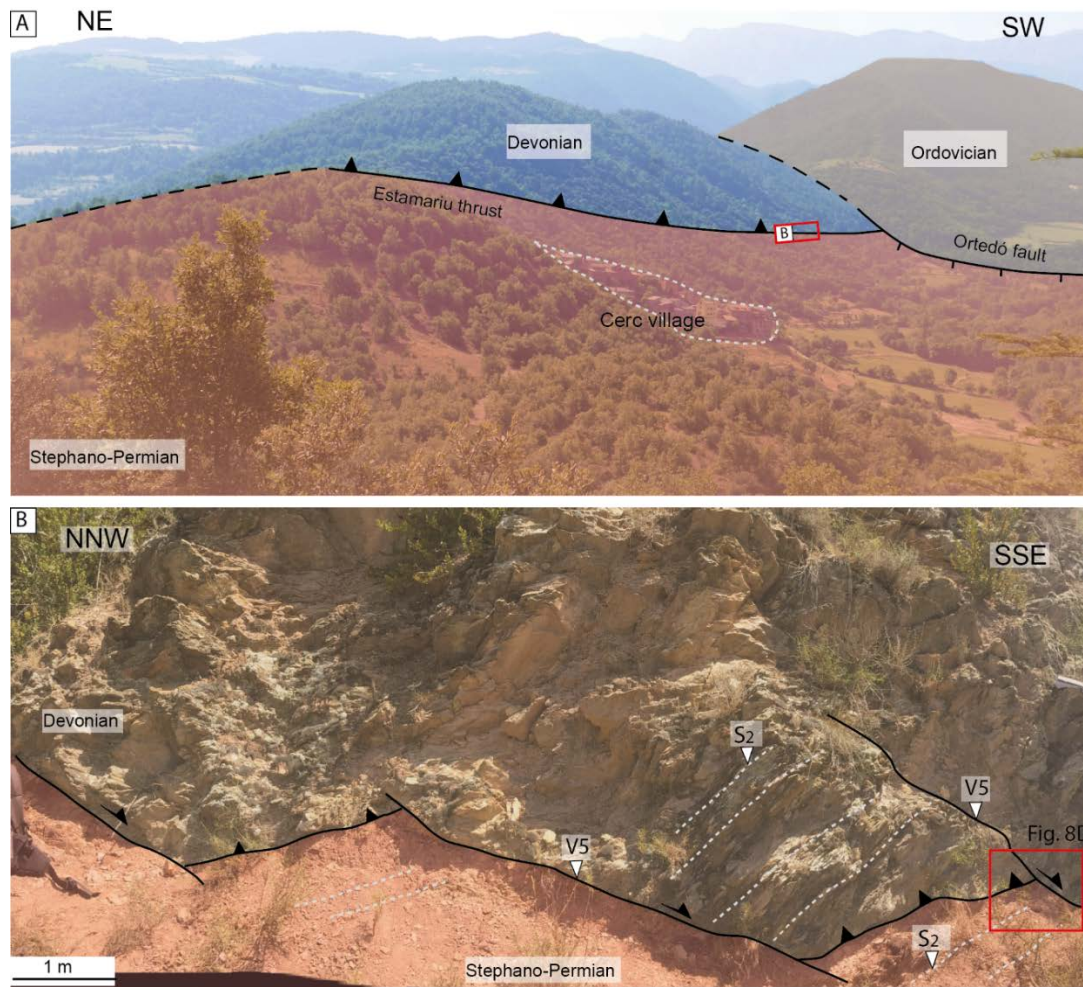
Figure 4: Main outcrop of the Estamariu thrust. A) Panoramic view from the Sant Antoni hill showing the extensional Ortedó fault postdating the Estamariu thrust. B) Main outcrop showing the Estamariu thrust and the related thrust zone foliation developed in the Devonian hanging wall and in the Stephano-Permian footwall (S_2). The thrust is displaced by later shear fractures locally mineralized with calcite (V5).

775
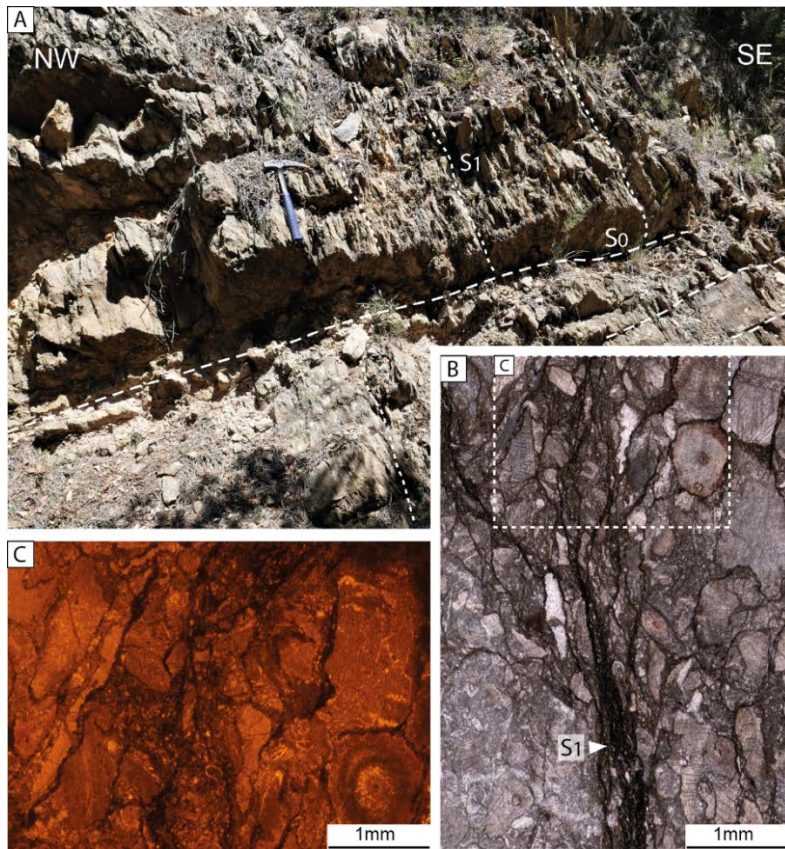
780

Figure 5: Devonian protolith. A) Field image showing the relationship between bedding (S_0) and regional foliation (S_1). B) Plane polarized light and C) Cathodoluminescence microphotographs of the encrinites alternating with pelitic rich bands, where the S_1 is concentrated.
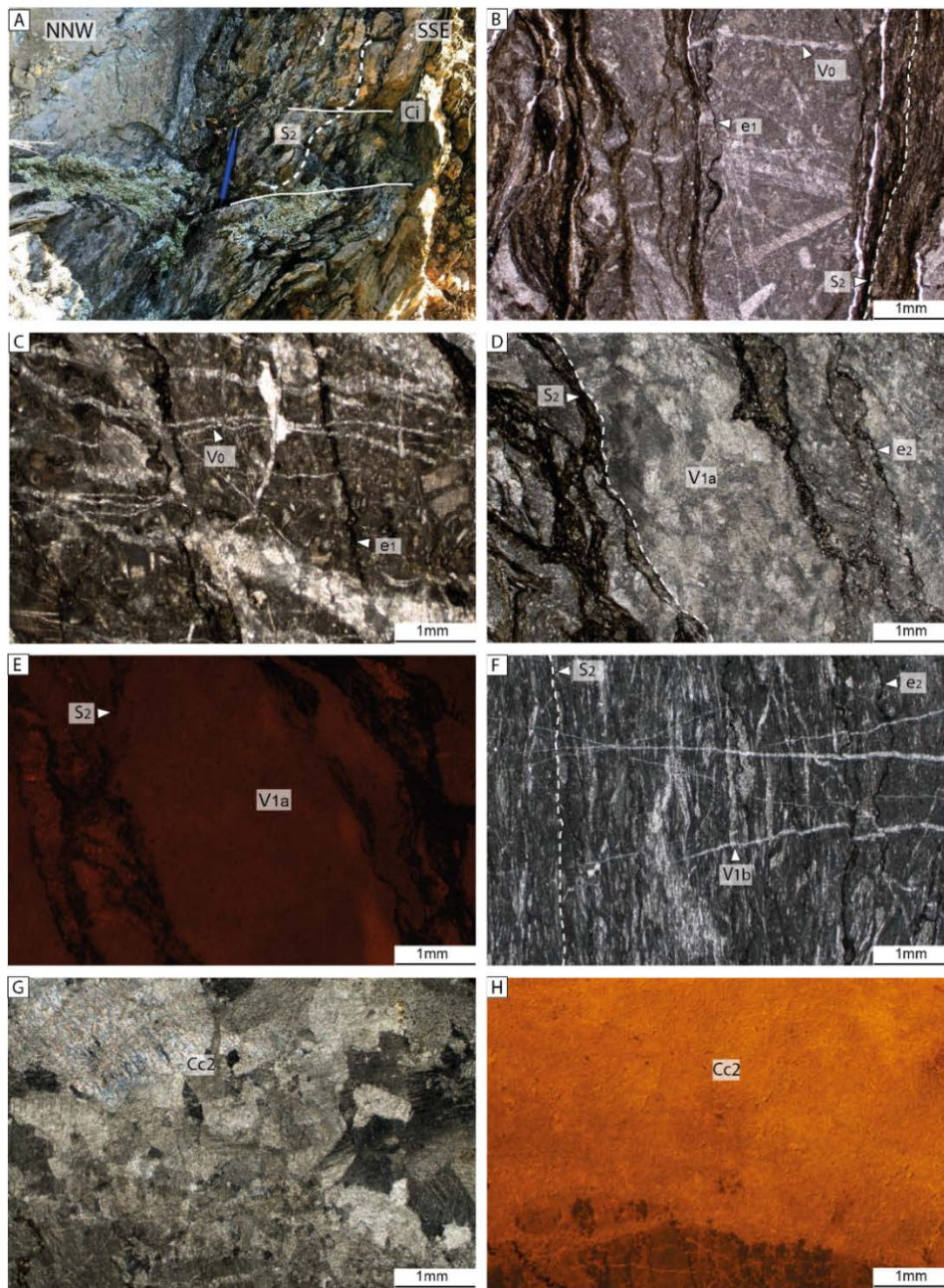
785

Figure 6: Mesostructures and microstructures found within the thrust zone affecting the hanging wall. A) Outcrop image of the thrust zone foliation (S_2) and related C planes indicating reverse kinematics (Ci). Microphotographs of B) thrust zone foliation (S_2), C) Stylolites e1 and veins V0 affecting the Devonian encrinites, D) Crossed polarized light and E) cathodoluminescence microphotographs of veins V1a concentrated between foliation surfaces. F) Thrust zone foliation (S_2) near the fault plane and
790 **ambiguous and perpendicular relationships between V1b and e2. G) Crossed polarized light and H) cathodoluminescence microphotographs of calcite cement Cc2 located on the main thrust plane (V2).**
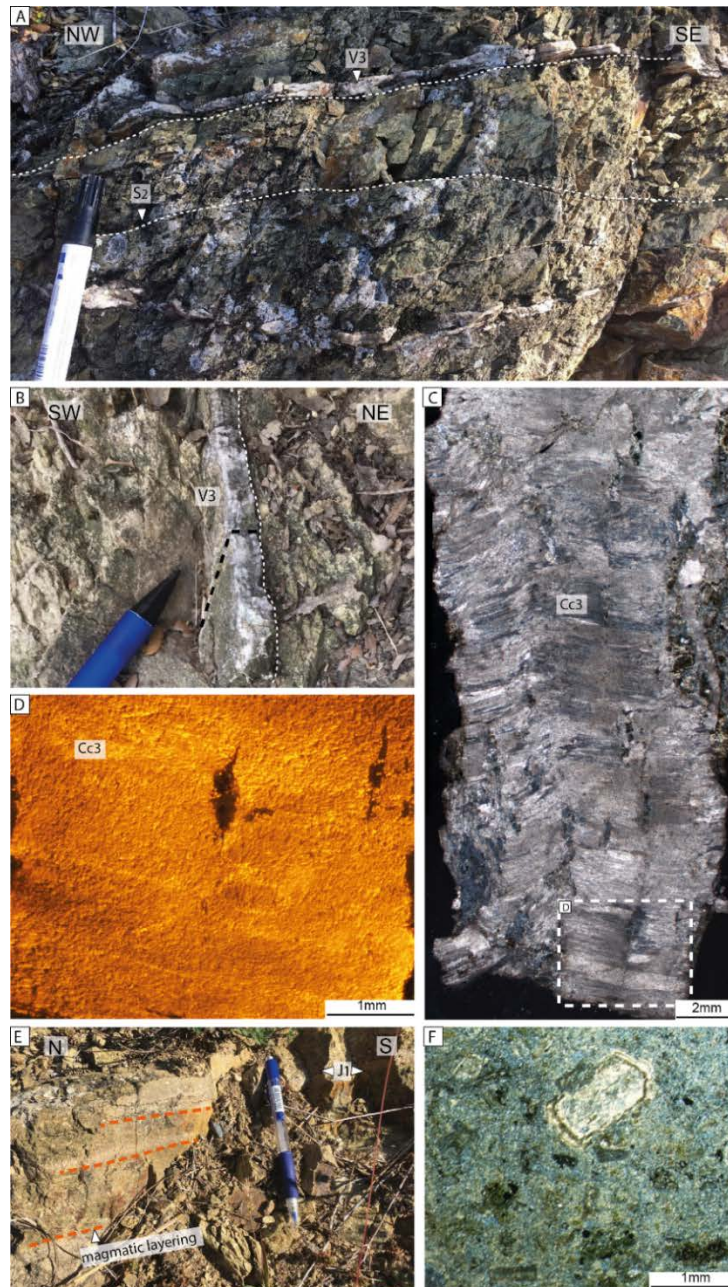
Figure 7: Mesostructures and microstructures present in the Stephano-Permian volcanic footwall. A) Field image of the subsidiary thrust zone in the footwall showing the thrust zone foliation (S_2) and the veins V3. B) Detail of veins V3 also in the subsidiary thrust zone. The black dashed line indicates the original position of the thin section observed in C. C) Crossed polarized light and D) Cathodoluminescence microphotographs of veins V3, characterized by calcite fibers growing perpendicular to the vein walls ($Cc3$). E) Field image of the footwall andesites showing the magmatic layering and joints J1. F) Plane polarized light microphotograph of the volcanic andesites exhibiting a porphyritic texture with a large plagioclase crystal.

795

800
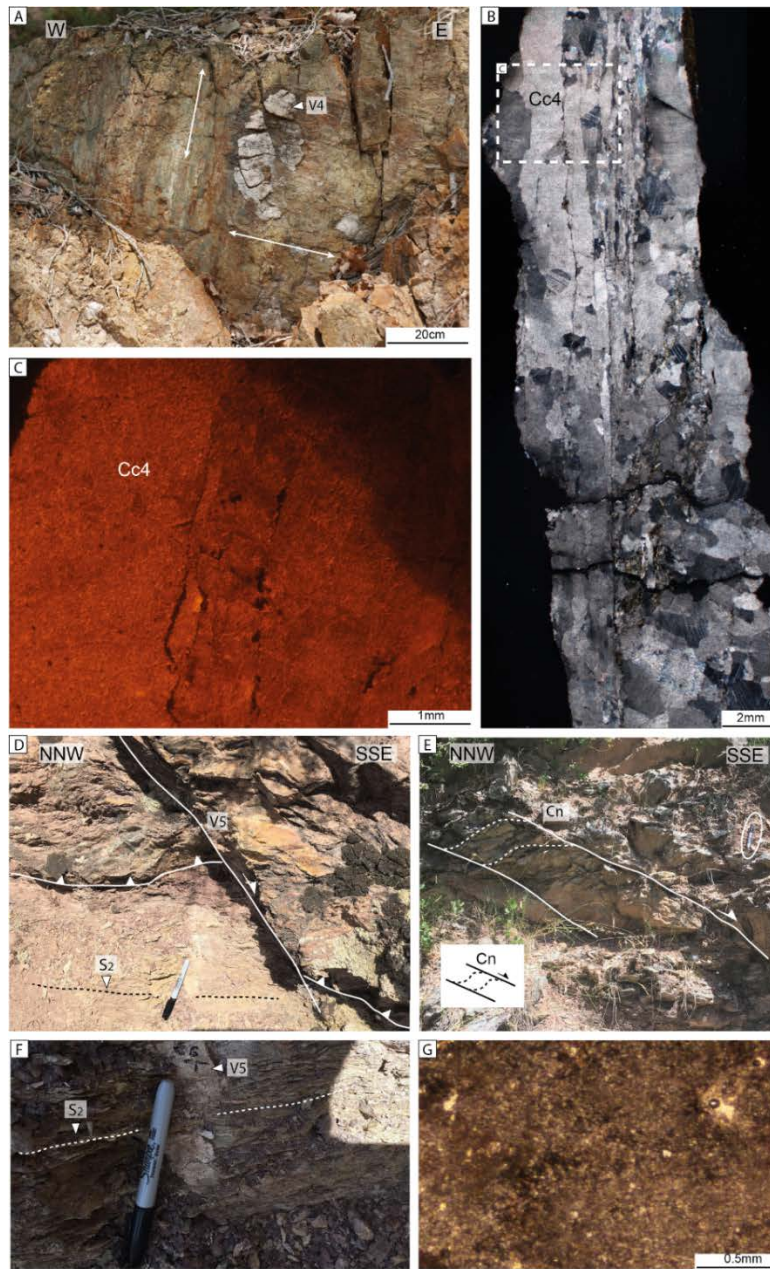
Figure 8: A) Field image of a subvertical and E-W fault plane mineralized with calcite (veins V4) and showing two striae set generations (white arrows) indicating dip-slip and strike-slip kinematics. B) Crossed polarized light and C) cathodoluminescence microphotographs of the vein-related calcite cement (Cc4). D) Shear fracture postdating the thrust zone foliation, locally

805 **mineralized with calcite veins V5. E) Shear bands (Cn) with normal kinematics located in the main thrust zone, indicating a later reactivation of the Estamariu thrust. (F) Field image of a calcite vein V5 and (G) Plane polarized light of the vein-related cement (Cc5).**

810
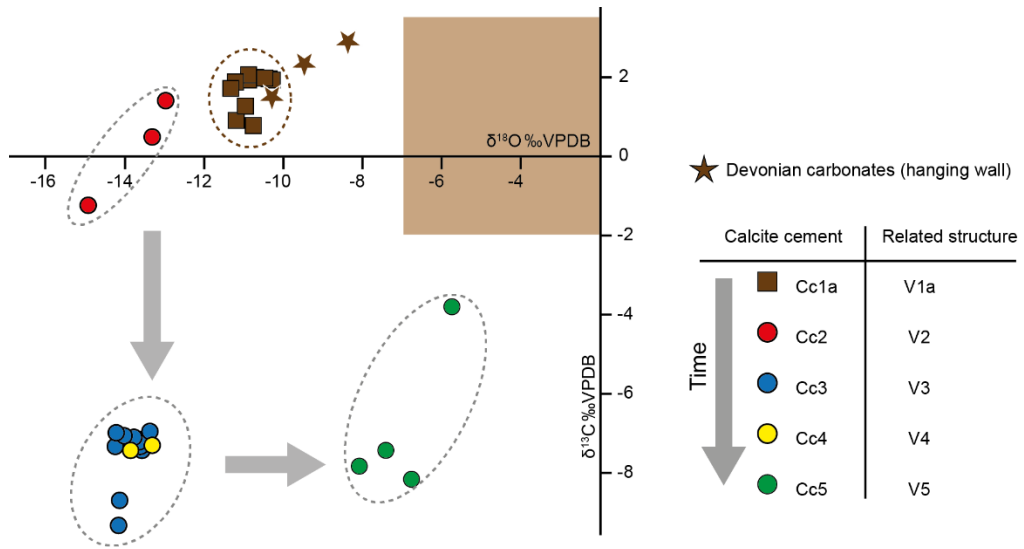
Figure 9: δ¹⁸O and δ¹³C values of calcite cements Cc1a to Cc5 and the Devonian carbonates from the hanging wall. Arrows indicate evolution over time according to the inferred relative timing of cements. The brown box refers to typical values of Devonian marine carbonates (Veizer et al., 1999).

815

820
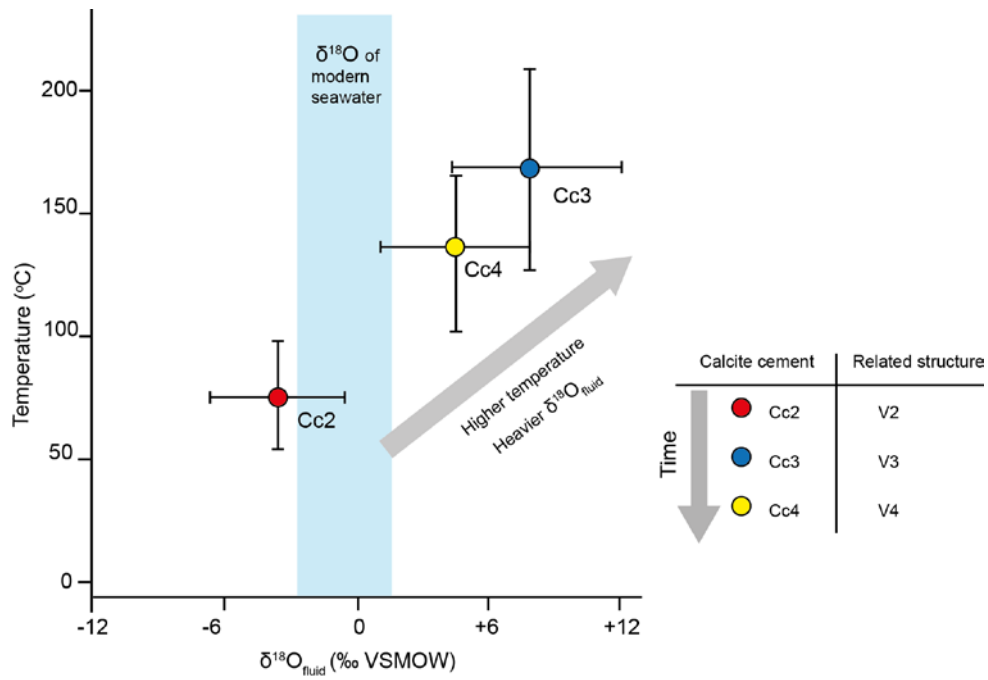
825

Figure 10: Temperatures (ºC) vs δ¹⁸O$_{fluid}$ calculated for cements Cc2 to Cc4. The typical δ¹⁸O values for modern seawater (blue band) are from (Veizer et al., 1999).
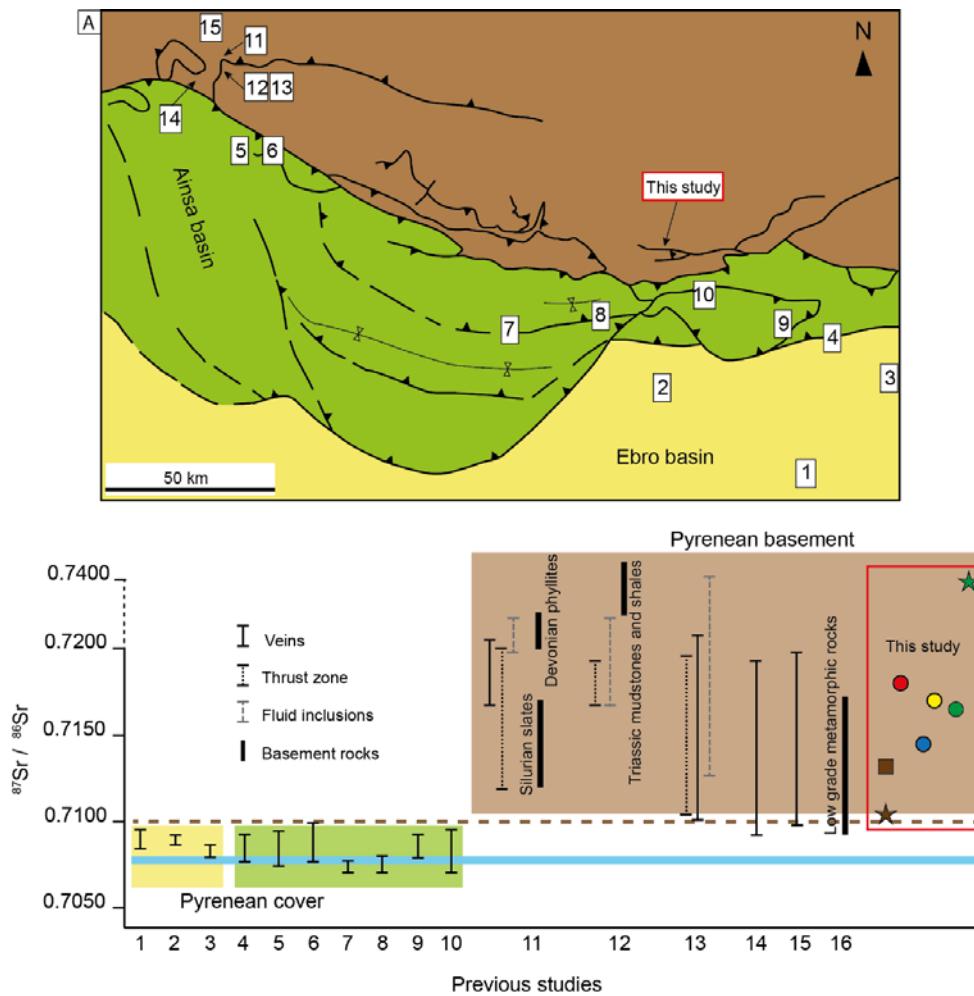
Figure 11: Simplified geological map of the south-central Pyrenees showing the location of structures where $^{87}Sr/^{86}Sr$ analysis have been carried out. Below, $^{87}Sr/^{86}Sr$ ratios from this study compared to results from other structures involving either cover units (1-10) or basement rocks (11-16). The blue thick line refers to the $^{87}Sr/^{86}Sr$ range of Phanerozoic seawater and the dashed brown line represents the $^{87}Sr/^{86}Sr$ limit value between basement and cover structures. 1. El Guix anticline (Travé et al., 2000), 2. Puig Reig anticline (Cruset et al., 2016), 3. L'Escala thrust (Cruset et al., 2018), 4.Vallfogona thrust (Cruset et al., 2018), 5. Ainsa basin (Travé et al., 1997), 6. Ainsa-Bielsa area (McCaig et al., 1995), 7. Minor Bóixols thrust (Muñoz-López et al., 2020), 8. Bóixols anticline (Nardini et al., 2019), 9. Lower Pedraforca thrust (Cruset et al., 2020a), 10. Upper Pedraforca thrust (Cruset, 2019), 11. Gavarnie thrust (McCaig et al., 1995), 12. Pic de Port Vieux thrust (Banks et al., 1991), 13. Pic de Port Vieux thrust (McCaig et al., 2000b), 14. Plan de Larri thrust (McCaig et al., 1995), 15. La Glere shear zone (Wayne and McCaig, 1998). 16. Trois Seigneurs Massif (not in the map) (Bickle et al., 1988).
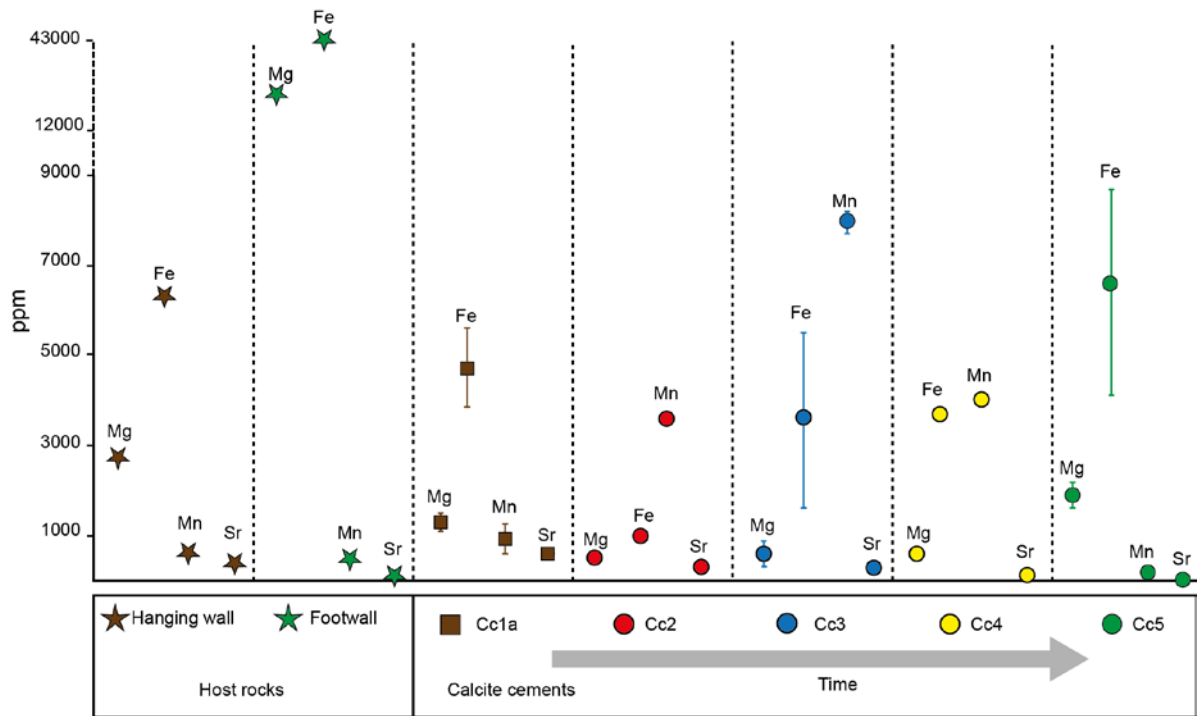
Figure 12: Elemental composition (including Mg, Fe, Mn and Sr) in ppm of the different calcite cements and host rocks. Bars indicate maximum, minimum and average composition.

A Alpine compression

Reactivation of the Estamariu thrust. Calcite cements Cc1a and Cc2

Estamariu thrust

← N

Legend:
- Unconformity
- Thrust
- Thrust zone
- Normal fault
- Neogene
- Stephano-Permian
- Devonian
- Upper Ordovician
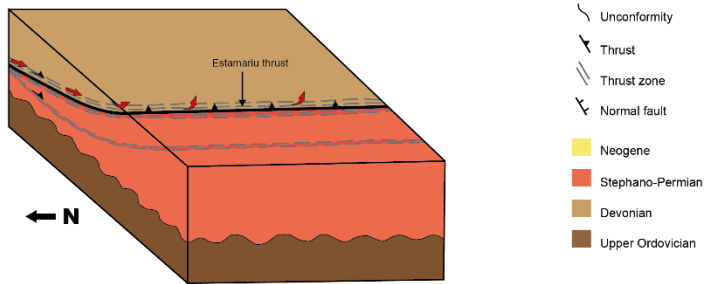
Regional tectonism	**A Alpine compression**		**B Neogene extension**		
Calcite cement	Cc1a	Cc2	Cc3	Cc4	Cc5
Related structure	V1a	V2	V3	V4	V5
Geochemistry	$\delta^{13}C_{calcite}$ +/−				
	$\delta^{18}O_{calcite}$ +/−				
	$^{87}Sr/^{86}Sr$ +/−				
	Mg +/−				
	Fe +/−				
	Mn +/−				
	Sr +/−				
	$\delta^{18}O_{fluid}$ +/−				
Temperature +/−					
Fluid source	Upward meteoric fluid		Upward hydrothermal fluid		Downward meteoric fluid
Implications	Change in the fluid regime. Increasing extent of fluid-rock interaction			Main change in the fluid regime	

B Neogene extension

Reactivation of the Estamariu thrust and development of normal faults
Calcite cement Cc3, Cc4 and Cc5

← N

La Seu d'Urgell fault

Ortedó fault
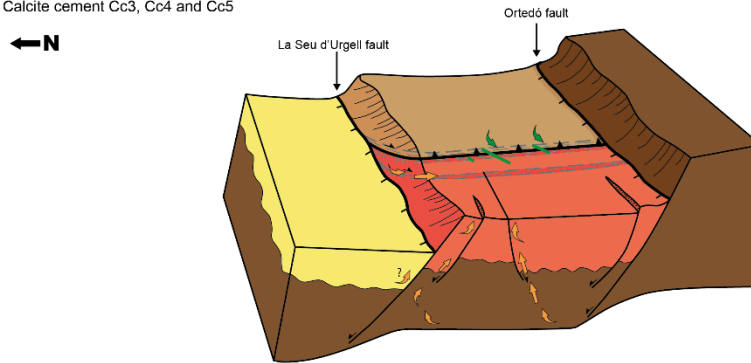
850

Figure 13: Tectonic and geochemical evolution of the study area (not to scale) and relationships with the evolution of the fluid system. A) During the Alpine reactivation of the Estamariu thrust, a meteoric fluid (red arrows) interacted at depth with basement rocks and then migrated along the fault plane towards the hanging wall, precipitating cements Cc1a and Cc2. B) During the Neogene extension, basement-derived hydrothermal fluids (orange arrows) flowed upwards through newly formed and reactivated
855 **fault zones. This fluid precipitated calcite cements Cc3 and Cc4. Finally, during ongoing deformation, meteoric fluids (green arrows) percolated in the system and precipitated Cc5, revealing a main change in the fluid regime.**